ARTICLE

Suppression of ventricular arrhythmias by targeting late L-type Ca^{2+} current

Marina Angelini[1]*[iD], Arash Pezhouman[2]*[iD], Nicoletta Savalli[1][iD], Marvin G. Chang[3], Federica Steccanella[1], Kyle Scranton[1], Guillaume Calmettes[2], Michela Ottolia[1,7][iD], Antonios Pantazis[4,5][iD], Hrayr S. Karagueuzian[2,6][iD], James N. Weiss[2,6,8][iD], and Riccardo Olcese[1,6,7,8][iD]

Ventricular arrhythmias, a leading cause of sudden cardiac death, can be triggered by cardiomyocyte early afterdepolarizations (EADs). EADs can result from an abnormal late activation of L-type Ca^{2+} channels (LTCCs). Current LTCC blockers (class IV antiarrhythmics), while effective at suppressing EADs, block both early and late components of $I_{Ca,L}$, compromising inotropy. However, computational studies have recently demonstrated that selective reduction of late $I_{Ca,L}$ (Ca^{2+} influx during late phases of the action potential) is sufficient to potently suppress EADs, suggesting that effective antiarrhythmic action can be achieved without blocking the early peak $I_{Ca,L}$, which is essential for proper excitation–contraction coupling. We tested this new strategy using a purine analogue, roscovitine, which reduces late $I_{Ca,L}$ with minimal effect on peak current. Scaling our investigation from a human Ca$_V$1.2 channel clone to rabbit ventricular myocytes and rat and rabbit perfused hearts, we demonstrate that (1) roscovitine selectively reduces $I_{Ca,L}$ noninactivating component in a human Ca$_V$1.2 channel clone and in ventricular myocytes native current, (2) the pharmacological reduction of late $I_{Ca,L}$ suppresses EADs and EATs (early after Ca^{2+} transients) induced by oxidative stress and hypokalemia in isolated myocytes, largely preserving cell shortening and normal Ca^{2+} transient, and (3) late $I_{Ca,L}$ reduction prevents/suppresses ventricular tachycardia/fibrillation in ex vivo rabbit and rat hearts subjected to hypokalemia and/or oxidative stress. These results support the value of an antiarrhythmic strategy based on the selective reduction of late $I_{Ca,L}$ to suppress EAD-mediated arrhythmias. Antiarrhythmic therapies based on this idea would modify the gating properties of Ca$_V$1.2 channels rather than blocking their pore, largely preserving contractility.

Introduction

Sudden cardiac death due to ventricular fibrillation (VF) is a worldwide public health problem estimated to account for 1–5 million deaths annually (Chugh et al., 2008; Cygankiewicz, 2020), with 300,000–450,000 cases in the US alone (Kong et al., 2011; George, 2013; Benjamin et al., 2018). VF is typically initiated by an abnormal electrical excitation of the myocardium associated with a premature ventricular complex (PVC). PVCs, which are events occurring at the tissue level, can be caused by oscillations of the cellular membrane potential, called early afterdepolarizations (EADs), that interrupt the normal repolarization phase of the cardiac action potential (AP), causing its prolongation. When EADs from a sufficiently large group of cells synchronize (Sato et al., 2009), they can cause triggered activity (and PVCs), torsades de pointes, polymorphic ventricular

tachycardia (VT), and VF (Cranefield and Aronson, 1991; Morita et al., 2009; Qu et al., 2013; Weiss et al., 2015; Wit, 2018). In addition, the AP prolongation caused by EADs may amplify the heterogeneity of tissue repolarization, predisposing the heart to reentrant tachyarrhythmias (Antzelevitch and Burashnikov, 2011). Therefore, EADs are a potent cellular-level abnormality of AP repolarization that can have dire consequences for cardiac function.

The L-type Ca^{2+} channel (LTCC) current ($I_{Ca,L}$) plays a prominent role in EAD formation and propagation (January et al., 1988; January and Riddle, 1989; Zeng and Rudy, 1995; Xie et al., 2009). Shortly after the AP upstroke, LTCCs activate rapidly, generating the early peak $I_{Ca,L}$ that triggers SR Ca^{2+} release (Bers, 2002; Eisner et al., 2017). While during an AP most

[1]Division of Molecular Medicine, Department of Anesthesiology & Perioperative Medicine, David Geffen School of Medicine, University of California, Los Angeles, Los Angeles, CA; [2]Department of Medicine (Cardiology), David Geffen School of Medicine, University of California, Los Angeles, Los Angeles, CA; [3]Department of Anesthesia and Critical Care, Massachusetts General Hospital, Harvard Medical School, Boston, MA; [4]Division of Neurobiology, Department of Biomedical and Clinical Sciences, Linköping University, Linköping, Sweden; [5]Wallenberg Center for Molecular Medicine, Linköping University, Linköping, Sweden; [6]Cardiovascular Research Laboratories, David Geffen School of Medicine, University of California, Los Angeles, Los Angeles, CA; [7]University of California, Los Angeles Cardiovascular Theme, David Geffen School of Medicine, University of California, Los Angeles, Los Angeles, CA; [8]Department of Physiology, David Geffen School of Medicine, University of California, Los Angeles, Los Angeles, CA.

*M. Angelini and A. Pezhouman contributed equally to this paper; Correspondence to Riccardo Olcese: rolcese@ucla.edu.

LTCCs undergo Ca^{2+}- and voltage-dependent inactivation (Brehm and Eckert, 1978; Kass and Sanguinetti, 1984; Lee et al., 1985; Peterson et al., 1999; Zühlke et al., 1999; Soldatov, 2012), a fraction of channels remains conducting, producing a persistent Ca^{2+} current that flows during the late phases of the AP: the late $I_{Ca,L}$. Late $I_{Ca,L}$ constitutes a relatively small but critical inward current influencing the amplitude and duration of the cardiac AP (Morotti et al., 2012; Qu and Chung, 2012). Under conditions of reduced repolarization reserve, the late $I_{Ca,L}$ can reverse the normal repolarization, contributing to membrane potential oscillations (i.e., EADs; January and Riddle, 1989; Antoons et al., 2007; Madhvani et al., 2011; Qu and Chung, 2012; Madhvani et al., 2015). Similar to late Na^+ channel current (Maltsev et al., 1998; Wagner et al., 2011; Banyasz et al., 2015; Chen-Izu et al., 2015; Bengel et al., 2017), enhanced late $I_{Ca,L}$ has been associated with augmented Ca^{2+}/calmodulin-dependent kinase II (CaMKII) activity and propensity to VT/VF (Xie et al., 2009; Song et al., 2010).

Late $I_{Ca,L}$ is the current conducted by channels that are in quasi–steady state (Fig. 1 A). Therefore, the behavior and extent of late $I_{Ca,L}$ are largely determined by the $I_{Ca,L}$ steady-state activation and inactivation curves. The overlapping of these two curves defines the "window current" region (Fig. 1): a range of membrane potentials in which LTCCs are not inactivated and are available for activation. Oxidative stress (experimentally mediated by H_2O_2 perfusion; Ward and Giles, 1997; Xie et al., 2009; Madhvani et al., 2011; Karagueuzian et al., 2013; Madhvani et al., 2015) facilitates LTCC activation by altering LTCC steady-state activation and inactivation properties, causing an overall widening of the $I_{Ca,L}$ window current region (Xie et al., 2009; Song et al., 2010; Madhvani et al., 2011; Yang et al., 2013). Prolongation of the AP increases the time when the membrane potential lingers within the $I_{Ca,L}$ window current voltage range, thus increasing the probability of inward $I_{Ca,L}$ to be flowing, causing EADs. It follows that a reduction of the window current region, achieved by altering $I_{Ca,L}$ steady-state properties, will reduce late $I_{Ca,L}$, consequently suppressing EADs and their arrhythmogenic effects (Madhvani et al., 2011; Qu and Chung, 2012; Madhvani et al., 2015). Under dynamic clamp, by injecting a virtual, tunable $I_{Ca,L}$ into isolated myocytes, we recently demonstrated that a potent EAD-suppressing action can be produced by decreasing the pedestal component of the LTCC steady-state inactivation curve, effectively reducing the $I_{Ca,L}$ window current region (Fig. 1; and Fig. S4, A–C; Madhvani et al., 2015; Markandeya and Kamp, 2015).

The efficacy of $I_{Ca,L}$ window current reduction as an anti-EAD strategy was recently confirmed by another dynamic-clamp study in atrial myocytes (Kettlewell et al., 2019), in a human anatomical computational model of long QT (LQT) syndromes (Liu et al., 2019), and in single-cell computational modeling (Qu and Chung, 2012; Kimrey et al., 2020), emphasizing the potency of this antiarrhythmic strategy. The abovementioned body of work supports a potentially groundbreaking antiarrhythmic strategy centered on the modulaton of $I_{Ca,L}$ window current that, unlike conventional LTCC blockers (class IV antiarrhythmics), does not block the LTCC channel but selectively reduces the late $I_{Ca,L}$, largely preserving contractility.

In the present study, we have tested and validated this idea: pharmacologically using roscovitine, a drug found to enhance voltage-dependent inactivation of LTCC channels (Yarotskyy and Elmslie, 2007; Yarotskyy et al., 2009; Yarotskyy et al., 2010; Yazawa et al., 2011), to effectively reduce the late $I_{Ca,L}$.

Remarkably, roscovitine preferentially decreases the late $I_{Ca,L}$ without affecting the peak $I_{Ca,L}$ (Yarotskyy and Elmslie, 2007; Yarotskyy et al., 2010), offering a unique opportunity to directly evaluate antiarrhythmic action associated with late $I_{Ca,L}$ reduction. We found that not only did roscovitine potently suppress EADs and EATs (early after Ca^{2+} transients) in isolated ventricular myocytes, but critically, it also suppresses and/or prevents EAD-mediated VT/VF in whole, isolated rabbit and rat hearts.

While roscovitine, a purine analogue, is not clinically appropriate as an antiarrhythmic drug due to its kinase-inhibiting activity, our results provide a proof of concept at the preclinical level for a new class of antiarrhythmic drugs, LTCC gating modifiers, for treating EAD-mediated VT/VF. Unlike current, conventional class IV antiarrhythmics, the antiarrhythmic action of LTCC gating modifiers is expected to largely preserve cardiac inotropy.

Materials and methods

Ethical approval
All animal protocols were approved by the University of California, Los Angeles (UCLA) Institutional Animal Care and Use Committee and conformed to the Guide for the Care and Use of Laboratory Animals published by the US National Institutes of Health.

Ventricular myocytes isolation
Hearts were removed from New Zealand young adult male rabbits (3–5 mo old) anesthetized by intravenous injection of 1,000 U heparin sulfate and 100 mg/kg sodium pentobarbital.

Ventricular myocytes were enzymatically isolated using a retrograde Langendorff perfusion system at 37°C. Nominally Ca^{2+}-free Tyrode's solution containing (in mM) 136 NaCl, 5.4 KCl, 0.33 NaH_2PO_4, 1 $MgCl_2$, 10 glucose, and 10 HEPES, pH 7.4, and supplemented with ≈1.4 mg/ml collagenase (type II; Worthington Biochemical) and 0.1 mg/ml protease (type XIV) was perfused for 25–30 min. The ventricular tissue was then rinsed and minced in a culture dish with Tyrode's solution containing 0.2 mM Ca^{2+}. $[Ca^{2+}]$ was gradually increased to 1.8 mM, and the cells were stored at room temperature and used within ∼8 h.

Patch clamp
Ventricular myocytes were patch-clamped in the whole-cell configuration in voltage- or current-clamp mode. Voltage-clamp recordings were performed using square voltage steps or a modified ventricular AP waveform (AP clamp), described below. 1–2 MΩ borosilicate pipettes (Warner Instruments) were fabricated using a P97 micropipette puller (Sutter Instrument).

Voltage-clamp and $I_{Ca,L}$ recordings
The intracellular (pipette) solution contained (in mM) 110 Cs-aspartate, 30 CsCl, 5 NaCl, 10 HEPES, 0.1–0.5 EGTA, 5 MgATP, 5 creatine phosphate, and 0.05 cAMP, pH 7.2.
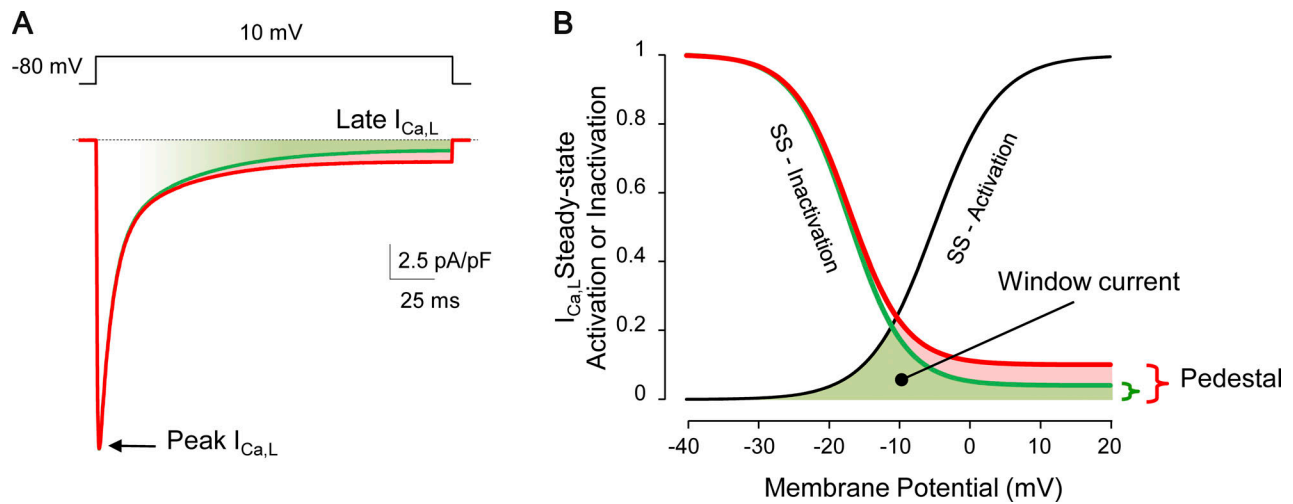
Figure 1. Proposed antiarrhythmic strategy based on the reduction of the late $I_{Ca,L}$ achieved by decreasing the pedestal component of the LTCC steady-state inactivation. (A) $I_{Ca,L}$ predictions for a depolarization to 10 mV (red trace) using a modified UCLA AP model (Madhvani et al., 2011; Madhvani et al., 2015). $I_{Ca,L}$ activates rapidly, generating a "peak," and inactivates incompletely, generating a small but sustained current that persists until the end of the depolarization (late $I_{Ca,L}$). Late $I_{Ca,L}$ is enhanced under pathological conditions (e.g., under oxidative stress, red trace; Madhvani et al., 2011), promoting EADs. As such, late $I_{Ca,L}$ represents an ideal target to suppress EAD-mediated arrhythmias (Madhvani et al., 2015). The antiarrhythmic strategy tested in this study is based on a reduction of the late $I_{Ca,L}$, as shown in A (green trace). **(A and B)** The two $I_{Ca,L}$ current traces (A) have been simulated using different parameter values for the $I_{Ca,L}$ steady-state (SS) inactivation (red curve = 10% pedestal; green curve = 4% pedestal) shown in B. In fact, as late $I_{Ca,L}$ flows in quasi–steady state, its amplitude is governed by the position and shape of the curves that describe its steady-state activation and inactivation properties (B). The area subtended by the overlapping steady-state activation and inactivation curves is traditionally referred to as the $I_{Ca,L}$ window current (B, color-filled area). A reduction of late $I_{Ca,L}$ (and $I_{Ca,L}$ window current) is achieved by lowering the $I_{Ca,L}$ steady-state inactivation pedestal component. Notably, lowering the $I_{Ca,L}$ pedestal (B) has no effect on the peak $I_{Ca,L}$ but it limits the amplitude of late $I_{Ca,L}$ (A).

Cells were superfused with a modified Tyrode's solution in which K$^+$ was replaced by Cs$^+$ to suppress K$^+$ conductance. This solution contains 1.8 mM Ca^{2+}. Na$_V$ channels were blocked by 10 μM extracellular tetrodotoxin (TTX) and inactivated by a 50-ms depolarization to −40 mV.

$I_{Ca,L}$ was isolated by subtracting the nifedipine-resistant current from the total current. The ionic currents were acquired in the absence or presence of 20 μM (R)-roscovitine (termed roscovitine throughout the manuscript).

$I_{Ca,L}$ steady-state activation curves were constructed by dividing the peak I-V data by the driving force. The data points were fitted to a Boltzmann function:

$$f(V) = \frac{1}{1 + \exp\left[\frac{zF}{RT}(Vhalf - Vm)\right]},$$

where z is the effective charge, $Vhalf$ is the half-activation potential, Vm is the membrane potential, F and R are the Faraday and gas constants, and T is the absolute temperature (294 K).

Steady-state inactivation curves were constructed from a typical double-pulse protocol by plotting the normalized peak current during a test pulse at +10 mV against conditioning pulses (200 ms) ranging from −40mV to +30 mV in 10-mV increments. Myocytes were held at −80-mV holding potential. The data points were fitted to a Boltzmann function:

$$f(V) = \frac{1 - pdest}{1 + \exp\left[\left(-\frac{zF}{RT}\right)(Vhalf - Vm)\right]} + pdest,$$

where $pdest$ represents the fraction of channel that does not inactivate, z is the effective charge, F and R are the Faraday and

gas constants, T is the absolute temperature, $Vhalf$ is the half-activation potential, and Vm is the membrane potential. The fitting parameters are reported in Table S1.

To characterize $I_{Ca,L}$ under AP clamp, a rabbit ventricular AP waveform was modified by immediately preceding its onset with a 50-ms depolarization to −40 mV to inactivate Na$_V$ channels and was used as a voltage command. The analytical procedure to isolate nifedipine-sensitive current under AP clamp is shown in Fig. S1. Briefly, to reconstruct the nifedipine-sensitive current in control and with 20 μM roscovitine, we subtracted the current after nifedipine from the current recorded at baseline and after roscovitine addition, respectively.

We have excluded from our analysis experiments where rundown was occurring during the first 5 min in whole-cell mode. All current recordings were done at room temperature.

Current-clamp recordings

APs were elicited by 2-ms-long supra-threshold depolarizing pulses.

The intracellular (pipette) solution contained (in mM) 110 K-aspartate, 30 KCl, 5 NaCl, 10 HEPES, 0.05–0.1 EGTA, 5 MgATP, 5 creatine phosphate, and 0.05 cAMP, pH 7.2.

The extracellular solution contained (in mM) 136 NaCl, 5.4 KCl, 0.33 NaH$_2$PO$_4$, 1.8 CaCl$_2$, 1 MgCl$_2$, 10 glucose, and 10 HEPES, pH 7.4.

Stable EAD regimes were induced by exposing the myocytes to oxidative stress (600 μM H$_2$O$_2$) or combining oxidative stress (100 μM H$_2$O$_2$) with hypokalemia (2 mM external K$^+$) using a pacing cycle length (PCL) of 6 s. These two stressors are known

Angelini et al.
Ca$_V$1.2 gating modification as antiarrhythmic strategy

Journal of General Physiology 3 of 17
https://doi.org/10.1085/jgp.202012584

to promote EADs by favoring Ca^{2+} and Na^+ overload and activating CaMKII (Xie et al., 2009; Pezhouman et al., 2015). These interventions, along with the long PCL that mimics a condition of bradycardia, favor the formation of a stable EAD regime (Xie et al., 2009; Madhvani et al., 2011; Madhvani et al., 2015; Nguyen et al., 2015; Pezhouman et al., 2015). 20 μM roscovitine was perfused (in the presence of the stressors) to study its effect on EADs. The reported AP voltages were corrected for liquid junction potentials. All current-clamp experiments were performed at 34–36°C.

AP duration at 90% repolarization (APD_{90}) and EAD occurrence (defined as percentage of APs that display a positive voltage deflection, dV/dt, of ≥5 mV; Fig. 4, Fig. 5, and Fig. 6) were reported as an average of seven consecutive APs measured at steady state (right before the start of the subsequent experimental condition).

All voltage- and current-clamp recordings were performed using an Axopatch 200B amplifier (Molecular Devices) and acquired using custom-made software (G-Patch; Analysis).

$Ca_V1.2$ clone and cut-open oocyte technique
Human α_{1C-77} subunits (GenBank accession no. CAA84346; Soldatov, 1992) of $Ca_V1.2$ channels with the auxiliary subunits $\alpha_2\delta$-1 (UniProt accession no. P13806) and β_{2b} (UniProt accession no. P54288) were coexpressed in *Xenopus laevis* oocytes. The complementary RNA of the different subunits was transcribed in vitro (AmpliCap-Max T7 High Yield Message Maker Kit; CELLSCRIPT) and injected into stage VI *Xenopus* oocytes (50 nl at 0.1–0.5 μg/μl). 3–4 d after injection, oocytes were voltage-clamped using the cut-open oocyte technique (Stefani and Bezanilla, 1998; Pantazis and Olcese, 2019). The ionic currents were acquired before and after the addition of 100 μM roscovitine at room temperature.

The external solution contained (in mM) 120 Na-methanesulfonate (MES), 2 $Ba(MES)_2$, and 10 HEPES, pH 7.0, supplemented with 0.1 ouabain to eliminate charge movement from Na/K adenosine triphosphatase (Neely et al., 1994).

The internal solution contained (in mM) 120 K-glutamate and 10 HEPES, pH 7.0.

The pipette solution contained (in mM) 2,700 Na-MES, 10 NaCl, and 10 Na-HEPES, pH 7.0. Before the experiments, oocytes were injected with 100 mM BAPTA•4K, pH 7.0 (2 × 50 nl), to prevent activation of native Ca^{2+}- and Ba^{2+}-dependent Cl^- channels (Barish, 1983).

The voltage dependence of channel opening (steady-state activation) and quasi–steady-state inactivation was determined using Boltzmann equations, as described above. The fitting parameters are reported in Table S2.

All recordings were performed using a CA-1 amplifier (DAGAN Corp.) and acquired using custom-made software (G-Patch).

Intracellular Ca^{2+} and cell shortening measurements
Changes in cytosolic $[Ca^{2+}]$ of rabbit ventricular myocytes were recorded from cells incubated for ≈20 min with 10 μM Ca^{2+} indicator Fluo-4 AM (Thermo Fisher Scientific) at room temperature. Cells were then washed, placed in a heated chamber on an inverted microscope, and field-stimulated by a pair of platinum electrodes carrying square-wave pulses of 2-ms duration, at 2 nA, every 5 or 6 s at 35°C. Intracellular calcium transients (Ca^{2+} transient) were recorded using scientific CMOS (Hamamatsu Photonics) or electron multiplying charge-coupled device (Princeton Instruments) cameras, operating at ≈50–100 frames/s.

Ventricular myocytes were paced for at least 2 min in Tyrode's solution before acquisition of the Ca^{2+} transients. EAT occurrence is presented as percentage of Ca^{2+} transients displaying EATs.

The Ca^{2+} transient amplitudes were calculated as $\Delta F/F0$. $\Delta F = Fmax - F0$, where Fmax is peak fluorescence intensity and F0 is fluorescence intensity before stimulation. Ca^{2+} transients shown in Fig. 7 D were acquired in control condition (Tyrode's) and after 2-min exposure (roscovitine suppresses EADs in <2 min; Fig. 4 A, Fig. 5 A, and Fig. 6 A) to either 20 μM roscovitine or DMSO 0.02% (vehicle).

The values of $\Delta F/F0$ in the presence of roscovitine or DMSO were normalized to the respective $\Delta F/F0$ of Ca^{2+} transients recorded before drug application and reported as the percentage of control (no-drug) condition. Ca^{2+} transient duration was measured as the full duration at half-maximal fluorescence amplitude.

Cell shortenings were measured in field-stimulated myocytes exposed to either 20 μM roscovitine or vehicle solution, as the percentage of shortening relative to resting cell length (% RCL) from acquired videos using ImageJ (Schneider et al., 2012).

Isolated perfused heart
To extensively evaluate the antiarrhythmic action of roscovitine, three ex vivo heart models were used: young and aged male Fisher344 rats (young: 3–4 mo old; aged: 22–24 mo old) and New Zealand young adult male rabbits (6–8 mo old). Hearts were isolated from anesthetized animals and perfused in a Langendorff apparatus at 37°C with Tyrode's solution containing (in mM) 125 NaCl, 24 $NaHCO_3$, 4.5 KCl, 1.8 NaH_2PO_4, 0.5 $MgCl_2$, 1.8 $CaCl_2$, and 5.5 glucose, pH 7.4, gassed with 95% O_2–5% CO_2. Aged rats have a high level of fibrosis in the heart tissue, a well-known pro-arrhythmic factor (Nguyen et al., 2014). In these ex vivo hearts, 100 μM H_2O_2 alone was sufficient to induce EAD-mediated VT/VF (Morita et al., 2009). In young rat hearts, arrhythmia was induced by hypokalemia (2 mM K^+; Pezhouman et al., 2015) as it was difficult to induce a stable arrhythmia using H_2O_2, possibly due to lower levels of fibrosis (Morita et al., 2009). In addition, the antiarrhythmic action of roscovitine was evaluated in adult rabbit, a species that has an AP morphology similar to that of human. In ex vivo rabbit hearts, a new model of arrhythmia was used, which comprises hypokalemia (1 mM K^+) combined with oxidative stress (100 μM H_2O_2). Spontaneously beating hearts were instrumented to continuously record local bipolar left-atrial and right-ventricular electrograms and a pseudo-electrocardiogram (p-ECG; Morita et al., 2009). Microelectrode recordings were obtained from the left ventricle as previously described (Morita et al., 2009; Morita et al., 2011a; Morita et al., 2011b; Bapat et al., 2012; Pezhouman et al., 2015). Recordings were acquired using a Digidata 1440A interface and Axoscope 10 software (Molecular Devices).

Chemicals and reagents

Chemicals and reagents were purchased from Sigma-Aldrich Co. unless otherwise indicated. (R)-roscovitine (LC Laboratories) was dissolved in either ethanol or DMSO to make a 100-mM stock solution. Final ethanol or DMSO concentrations never exceeded 0.1%. TTX was from Tocris Bioscience.

Data and statistical analysis

Data are presented as means ± SEM. n is the number of experimental replicates, and N indicates the number of animals. Box plots indicate first and third quartiles, median (red line), and mean (X); whiskers indicate 5 and 95 percentiles. Statistical significance was determined using two-tailed paired or unpaired Student's t tests and log-rank (Mantel-Cox) test for the Kaplan–Meier plot.

Online supplemental material

Fig. S1 shows the experimental and analytical procedure to isolate nifedipine-sensitive current under AP clamp in ventricular myocytes. Fig. S2 shows that roscovitine reduces late $I_{Ca,L}$ in human $Ca_V1.2$ channels. Fig. S3 shows that roscovitine suppresses hypokalemia-induced VT/VF in young rat hearts. Fig. S4 shows that $I_{Ca,L}$ pedestal reduction selectively reduces late versus peak $I_{Ca,L}$, unlike class-IV antiarrhythmics. Table S1 lists fitting parameters ± SEM of $I_{Ca,L}$ steady-state activation and inactivation in ventricular myocytes (control versus roscovitine). Table S2 lists fitting parameters ± SEM of $I_{Ca,L}$ steady-state activation and inactivation for human $Ca_V1.2$ complex expressed in oocytes (control versus roscovitine).

Results

Roscovitine selectively reduces late $I_{Ca,L}$ in rabbit ventricular myocytes without affecting peak current

Changes in the $I_{Ca,L}$ properties that increase the window current (Fig. 1) have been associated with an increased susceptibility to EADs and arrhythmia (e.g., LQT; January and Riddle, 1989; Antoons et al., 2007; Qi et al., 2009; Madhvani et al., 2011; Qu and Chung, 2012; Madhvani et al., 2015; Kettlewell et al., 2019; Liu et al., 2019). To evaluate the ability of roscovitine to reduce $I_{Ca,L}$ window current by limiting the late $I_{Ca,L}$, we first studied its action on native $I_{Ca,L}$ in rabbit ventricular myocytes exposed to oxidative stress (600 μM H_2O_2) to enhance late $I_{Ca,L}$. In fact, H_2O_2 exposure was shown to alter $I_{Ca,L}$ steady-state activation and inactivation properties, causing an overall widening of the $I_{Ca,L}$ window current region (Madhvani et al., 2011).

Under voltage clamp, we measured nifedipine-sensitive Ca^{2+} currents in the absence (Fig. 2 A) and in the presence (Fig. 2 B) of extracellular 20 μM roscovitine, and we found that roscovitine significantly reduced the late $I_{Ca,L}$ (noninactivating component at the end of the 200-ms depolarization), leaving the $I_{Ca,L}$ peak unperturbed (Fig. 2 C).

The effect of roscovitine on the $I_{Ca,L}$ window current can be well appreciated from the steady-state inactivation curve, which displays a significant reduction of the noninactivating component (pedestal) for potentials above –10 mV (Fig. 2 D, green triangles versus black diamonds). For example, the fraction of

noninactivating $I_{Ca,L}$ following a depolarization to 10 mV was reduced from 12% ± 1% to 3% ± 1% in the presence of 20 μM roscovitine (P = 0.0001, two-tailed unpaired t test; Fig. 2 D, green triangle versus black diamond). The roscovitine effect on $I_{Ca,L}$ was not associated with substantial changes in the voltage dependence of activation or inactivation (see Table S1).

Finally, we investigated the effect of roscovitine on late $I_{Ca,L}$ during an AP using a modified AP waveform as a voltage command for AP-clamp experiments. Roscovitine reduced the amplitude of Ca^{2+} current flowing during the late phases of the AP, minimally affecting peak $I_{Ca,L}$ (Fig. 3 A and Fig. S1). On average, 20 μM roscovitine had no significant effect on the peak current (3% ± 2% reduction, P = 0.083) but significantly reduced late $I_{Ca,L}$ by 25% ± 5%, (P = 0.001, measured at 150 ms during the AP clamp; Fig. 3 B). These results demonstrate that roscovitine selectively suppresses native late $I_{Ca,L}$ in ventricular myocytes also during a physiological stimulus. This selective action on late $I_{Ca,L}$ is expected to suppress EADs sustained by exaggerated activation of $I_{Ca,L}$ during phases 2 and 3 of the AP (Madhvani et al., 2011).

Roscovitine modifies the human $Ca_V1.2$ gating properties, reducing the late current with minimal effect on peak current

As the study of roscovitine has the potential to direct the development of derivatives with selective antiarrhythmic potency, we have evaluated its activity on the human $Ca_V1.2$ channel, assembled with $\alpha_2\delta$-1 and β_{2b}, the accessory subunits most abundantly expressed in the human heart (Hullin et al., 2003). Following the expression of this macromolecular complex in *Xenopus* oocytes, we found that extracellular application of roscovitine (100 μM) accelerated the rate of voltage-dependent inactivation, effectively reducing the noninactivating component or late $I_{Ca,L}$ with negligible effect on the peak current (Fig. S2 A). Roscovitine-induced reduction of human $Ca_V1.2$ window current is evident in the quasi–steady-state inactivation curve, which approached values close to zero in roscovitine-modified channels (Fig. S2 B). Roscovitine had practically no effect on the voltage dependence of activation and/or inactivation (see *Vhalf* of the steady-state curves in Fig. S2 B and Table S2). Thus, the roscovitine effect on the human clone closely recapitulated the effects we observed on the rabbit native ventricular $I_{Ca,L}$ (Fig. 2) and previously reported for the rabbit $Ca_V1.2$ clone (Yarotskyy and Elmslie, 2007; Yarotskyy et al., 2010).

Extracellularly applied roscovitine suppresses EADs of different etiologies in isolated rabbit ventricular myocytes

We postulated that drugs reducing the late $I_{Ca,L}$ should suppress EADs (Madhvani et al., 2015). As roscovitine selectively reduced late $I_{Ca,L}$ (Fig. 2, Fig. 3, and Fig. S2), we evaluated its efficacy at suppressing EADs in rabbit ventricular myocytes. We recorded cardiac APs at a PCL of 6 s, a condition of bradycardia that, in combination with oxidative stress (600 μM H_2O_2), favors the initiation of a stable EAD regime (Xie et al., 2009; Madhvani et al., 2011; Madhvani et al., 2015; Nguyen et al., 2015). Under these conditions, EADs appeared in 85.4% ± 4.1% of the APs, prolonging the APD_{90} from 246 ± 30 ms to 910 ± 121 ms. The addition of roscovitine (20 μM) to the extracellular solution suppressed H_2O_2-induced EADs in all myocytes tested and
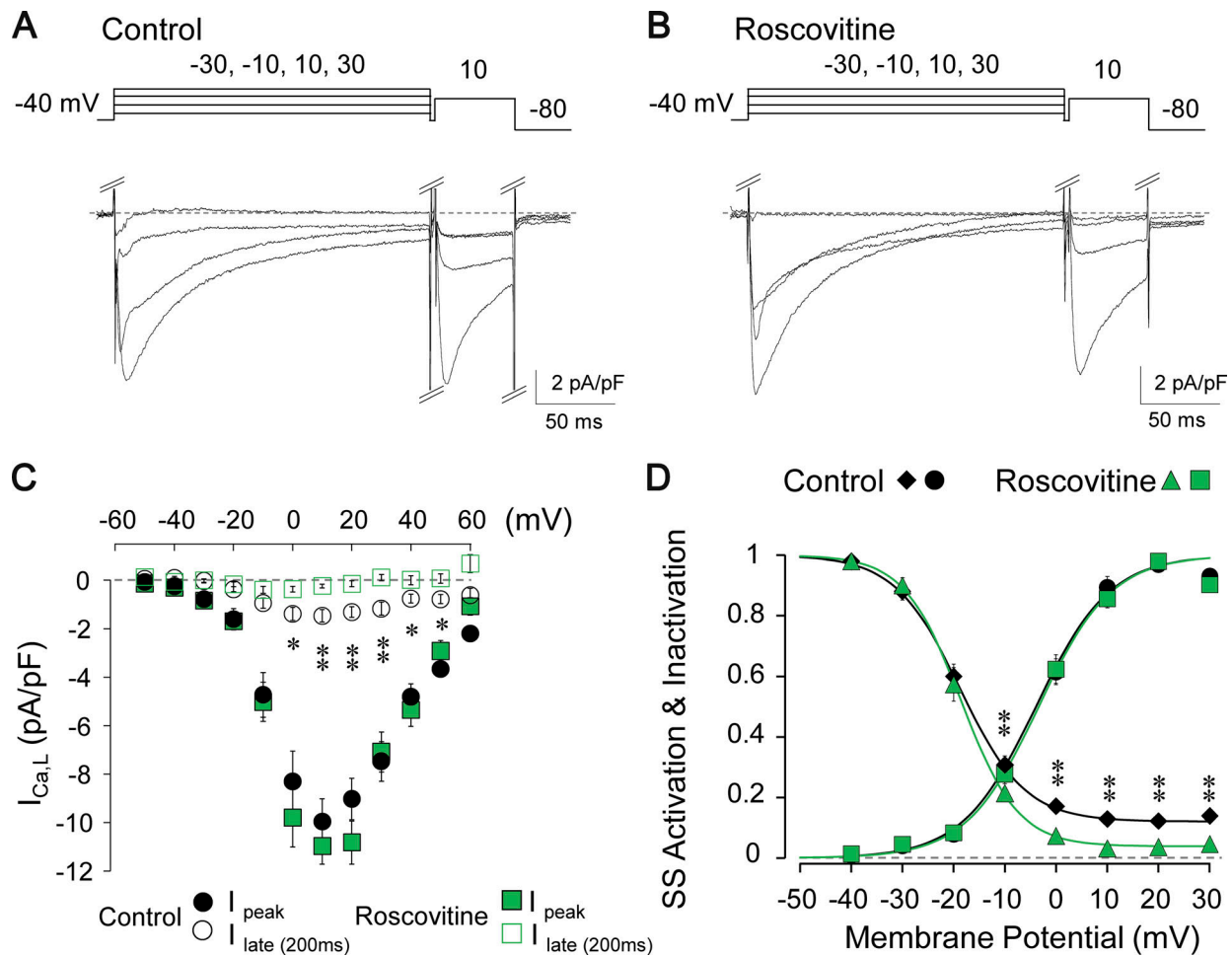
Figure 2. Roscovitine selectively reduces the late $I_{Ca,L}$ in rabbit ventricular myocytes without affecting $I_{Ca,L}$ peak. (A and B) Representative nifedipine-sensitive $I_{Ca,L}$ recordings elicited in response to the voltage protocol shown above (HP = −80 mV) in the presence of 600 µM H_2O_2 (control; A) or in the presence of 20 µM roscovitine + H_2O_2 (roscovitine; B). **(C)** Current-voltage relationship for peak and late $I_{Ca,L}$ (measured at the end of 200-ms depolarizations) in control (n = 6, N = 6; n/N refers to cells/animals measured in each group) and with 20 µM roscovitine (n = 6, N = 6). **(D)** $I_{Ca,L}$ steady-state (SS) activation and inactivation curves in control (n = 8, N = 6) and in the presence of roscovitine (n = 7, N = 6). Data points are mean ± SEM. Vertical asterisks, P < 0.001; *, P < 0.05.

restored normal APD_{90} (232 ± 25 ms), despite the continuous presence of H_2O_2 (Fig. 4; control APD_{90} versus roscovitine APD_{90}, P = 0.740, two-tailed unpaired t test). Under identical conditions, the perfusion of roscovitine vehicle (0.02% ethanol) had no significant effect on APD_{90} (Fig. 4 C; H_2O_2 versus vehicle, P = 0.646, two-tailed unpaired t test) and EAD regime (Fig. 4 C; H_2O_2 versus vehicle, P = 0.444, two-tailed unpaired t test).

To further test the robustness of the "anti-EAD" effect of roscovitine, we added an additional stressor, combining oxidative stress (100 µM H_2O_2) with hypokalemia (2 mM K^+). Reduced serum $[K^+]$ (hypokalemia) is a clinically relevant condition known to cause significant QT interval prolongation with subsequent risk of promoting lethal cardiac arrhythmias among cardiac patients (Osadchii, 2010; Weiss et al., 2017; Skogestad and Aronsen, 2018). The proarrhythmic action of hypokalemia is mainly due to the suppression of K^+ channel conductance (Sanguinetti and Jurkiewicz, 1992) and the inhibition of Na^+-K^+ adenosine triphosphatase, resulting in AP prolongation and reduced repolarization reserve along with

progressive cellular Na^+ and Ca^{2+} overload (Eisner et al., 1978; Pezhouman et al., 2015; Tazmini et al., 2020).

In isolated ventricular myocytes, the perfusion of this dual-stressor solution (H_2O_2 + hypokalemia) caused a hyperpolarization of the diastolic membrane potential from approximately −80 mV to approximately −110 mV, increased APD_{90} from 236 ± 34 ms to 772 ± 156 ms, and induced a stable EAD regime such that 97.6% ± 2.4% of the APs displayed at least one EAD within 6.7 ± 3.4 min (Fig. 5). Extracellularly perfused roscovitine (20 µM) completely suppressed EADs and decreased APD_{90} toward normal levels (304 ± 33 ms; Fig. 5; control versus roscovitine, P = 0.202, two-tailed paired t test) in the continuous presence of the stressors. Thus, pharmacological reduction of late $I_{Ca,L}$, brought about by roscovitine, can effectively suppress EADs in isolated ventricular myocytes (Fig. 4 and Fig. 5). We also found that the EAD-suppressing action of roscovitine is reversible: following roscovitine washout from the bath solution, EADs reappeared within minutes and could be suppressed by a second application of roscovitine (Fig. 5, A and B). On the other hand, intracellular
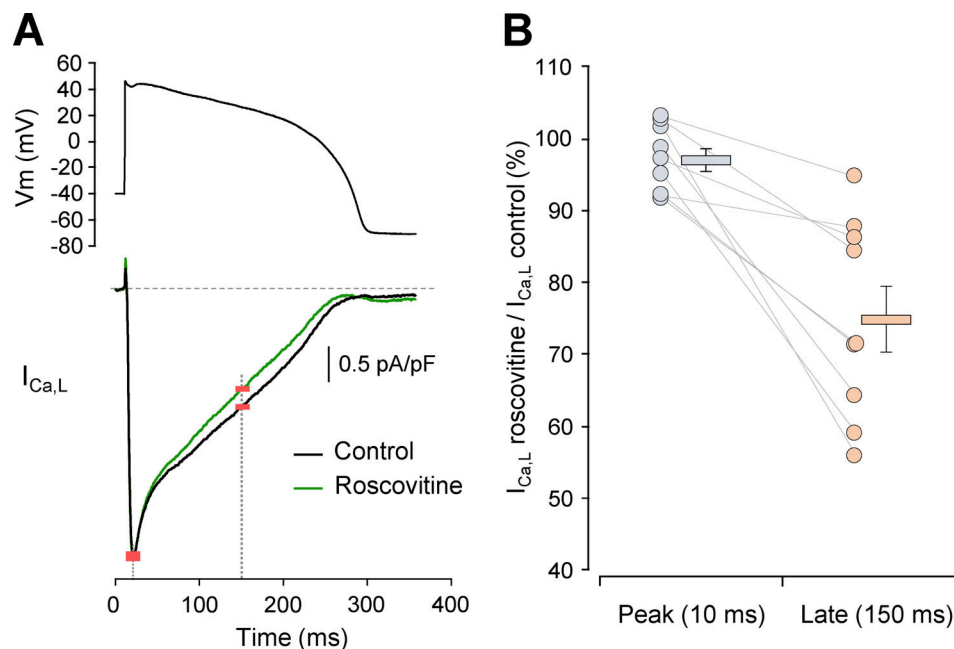
Figure 3. **Roscovitine selectively reduces the late $I_{Ca,L}$ in rabbit ventricular myocytes under AP clamp. (A)** Nifedipine-sensitive current ($I_{Ca,L}$) recorded before (black, control) and after 20 µM roscovitine (green) from the same myocytes under AP clamp. All recordings were performed in the presence of 600 µM H_2O_2. The vertical dotted lines indicate the times (10 ms and 150 ms) at which the extent of roscovitine reduction of the current was calculated. **(B)** Plot summarizing the extent of peak and late $I_{Ca,L}$ reduction caused by extracellular application of 20 µM roscovitine estimated from experiments as in A. Note that roscovitine selectively reduced the late $I_{Ca,L}$ without affecting peak $I_{Ca,L}$. Data points are mean ± SEM. $n = 9$, $N = 7$.

application of roscovitine failed to prevent the occurrence of EADs, suggesting an extracellular site of action. We dialyzed isolated myocytes with 20 µM roscovitine, carried by pipette intracellular solution (Fig. 6). After the rupture of the membrane patches and application of positive pressure to the patch pipette, the myocytes were paced at PCL = 6 s for ~8 min to allow for the diffusion of roscovitine into the cytoplasm. The presence of intracellular roscovitine did not prevent H_2O_2-induced EADs or AP prolongation, and EADs appeared within 7.3 ± 1.4 min. APD_{90} increased from 250 ± 16 ms in Tyrode's solution to 860 ± 200 ms in the presence of H_2O_2, with 76.2% ± 8.0% of APs showing EADs (Fig. 6 C). These effects are similar to those observed in the absence of intracellular roscovitine (Fig. 4 and Fig. 5). However, in these myocytes, the extracellular application of 20 µM roscovitine rapidly suppressed EADs and restored normal APD_{90} levels (211 ± 17 ms; Fig. 6 C; black square versus green dot, P = 0.230, two-tailed paired t test). The washout of roscovitine from the bath solution caused AP prolongation and reappearance of a stable EAD regime, which could also be suppressed by a second application of roscovitine (Fig. 6, A and B).

Together, these findings are consistent with the existence of an extracellular site for the EAD-suppressing action of roscovitine; this view is also in agreement with other studies that found that roscovitine exerts its effect by binding extracellularly to the repeat-I of $Ca_V1.2$ (Yarotskyy and Elmslie, 2007; Yarotskyy et al., 2010).

Roscovitine normalizes oxidative stress–induced EATs in ventricular myocytes
H_2O_2 has been shown to alter intracellular Ca^{2+} and cell contraction (Goldhaber and Liu, 1994; Greensmith et al., 2010).

Furthermore, previous studies have revealed that in electrically stimulated rabbit ventricular myocytes, H_2O_2 causes Ca^{2+} oscillations during the late phase of the Ca^{2+} transient; these events have been associated with EADs and reported as EATs (Xie et al., 2009; Zhao et al., 2012; Li et al., 2013). While the data in Fig. 4, Fig. 5, and Fig. 6 show that roscovitine corrects abnormal electrical signaling abolishing an EAD regime, it remains to be established whether it also corrects aberrant Ca^{2+} transients promoted by oxidative stress. In field-stimulated ventricular myocytes loaded with Ca^{2+} indicator Fluo-4 AM, the exposure to 200–600 µM H_2O_2 produced aberrant Ca^{2+} transients displaying EATs within minutes (Fig. 7 A). The addition of roscovitine (20 µM or 40 µM) to the extracellular solution significantly reduced the incidence of EATs in Ca^{2+} transients from 86% ± 3% to 15% ± 6% despite the persistent presence of H_2O_2 (Fig. 7, A and B; P < 0.001, two-tailed paired t test). The beneficial effect of roscovitine on EATs is likely to derive from its EAD-suppressing action associated with late $I_{Ca,L}$ reduction.

Roscovitine reduces late $I_{Ca,L}$ without affecting Ca^{2+} transients and cell shortening in isolated rabbit ventricular myocytes
A recognized limitation of current class IV antiarrhythmics (LTCC blockers), which reduces their clinical value, is their negative inotropic effect (Elliott and Ram, 2011). This drawback is directly related to their pore-blocking action on the $Ca_V1.2$ channel that produces overall reduction of the Ca^{2+} influx, equally affecting both peak and late $I_{Ca,L}$, resulting in decreased contractility. Since roscovitine suppressed EADs without reducing peak $I_{Ca,L}$ (Fig. 2, Fig. 3, and Fig. 4), we expected minimal effects on contractility and Ca^{2+} transient, which largely depend
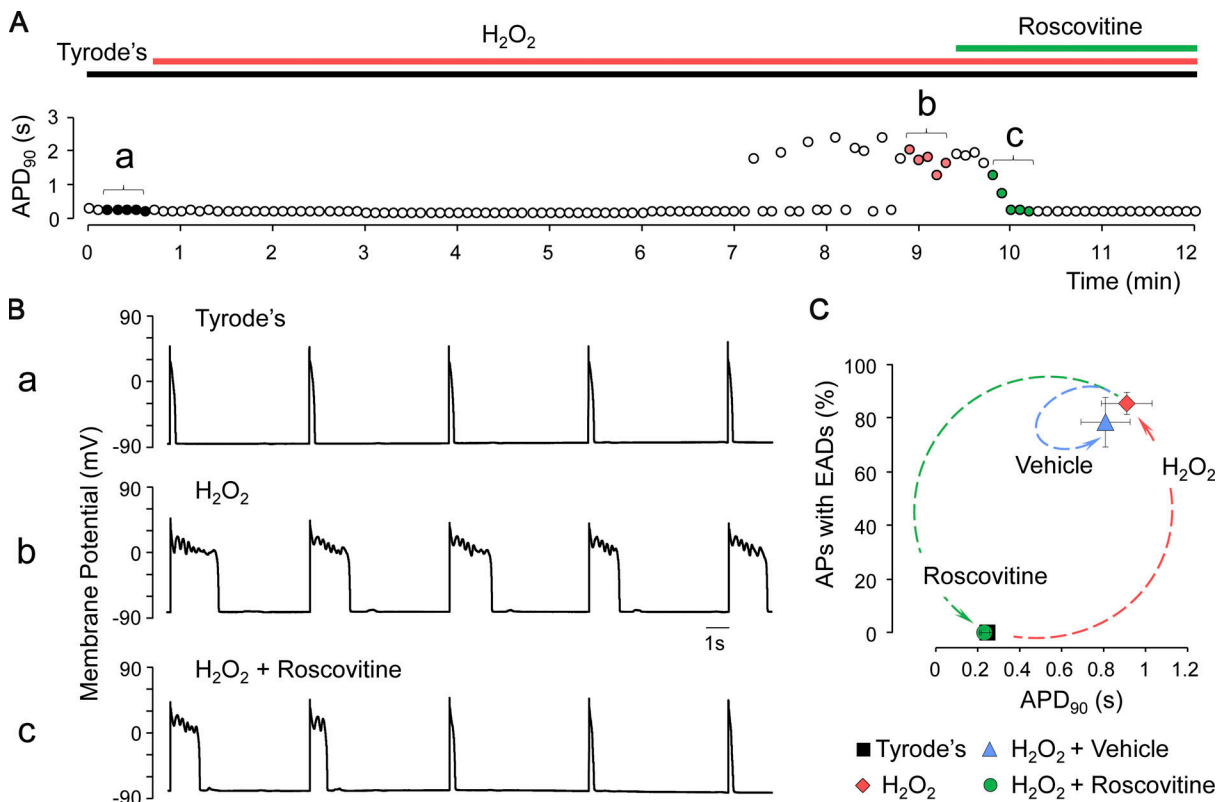
Figure 4. **Roscovitine suppresses oxidative stress–induced EADs in ventricular myocytes. (A and B)** Time course of APD_{90} (A) and selected APs (B) from the same myocyte for a representative experiment testing the EAD-suppressing action of roscovitine. A, a and B, a show AP recordings in control condition (Tyrode's solution). H_2O_2 perfusion (600 µM) induced a robust EAD regime (B, b) indicated by the sudden and dramatic increases of APD_{90} (A, b; ~6 min after H_2O_2 application). Extracellular addition of roscovitine (20 µM) completely abolished EAD occurrence and restored the normal AP duration despite the continuous presence of H_2O_2 (A, c and B, c). **(C)** Plot summarizing the average changes in APD_{90} and EAD occurrence during experiments performed as in A. Note that roscovitine suppressed EADs and restored a normal APD_{90}, unlike vehicle alone (0.02% ethanol, light blue triangle), which had no significant effect on the EAD regime (roscovitine: $n = 7$, vehicle: $n = 4$, $N = 9$; mean ± SEM).

on peak $I_{Ca,L}$. In fact, roscovitine did not alter resting cell length ($RCL_{vehicle}$: 126.1 ± 4.8 µm, $n = 21$; $RCL_{roscovitine} = 126.9 ± 4.6$ µm, $n = 24$; P = 0.907, two-tailed unpaired t test) or cell shortening (vehicle: 9.0% ± 0.83%; roscovitine: 9.22% ± 0.73%; P = 0.840, two-tailed unpaired t test), as shown in Fig. 7 C. In agreement with these data, roscovitine at the concentration that suppressed EADs (Fig. 4, Fig. 5, and Fig. 6) did not significantly alter Ca^{2+} transient duration in cells exposed to roscovitine compared with vehicle solution (Fig. 7, D and E; duration at half-maximal amplitude: vehicle: 279 ± 22 ms; roscovitine: 280 ± 15 ms; P = 0.955, two-tailed unpaired t test). However, roscovitine caused a small but statistically significant reduction of the Ca^{2+} transient amplitude (ΔF/F0) compared with ΔF/F0 reduction caused by the vehicle (DMSO; Fig. 7 F; vehicle: 93.89% ± 1.43%; roscovitine: 88.74% ± 1.23%; P = 0.01, two-tailed unpaired t test). Based on these results, we speculate that the antiarrhythmic (EAD-suppressing) action of late $I_{Ca,L}$ is unlikely to be complicated by negative inotropy, highlighting a potential advantage of $Ca_V1.2$ gating modifiers over class IV antiarrhythmics.

Assessing the antiarrhythmic potential of late $I_{Ca,L}$ reduction in ex vivo hearts
The data reported so far offer strong evidence that pharmacological reduction of late $I_{Ca,L}$ potently suppresses EADs in

isolated myocytes. In the next series of experiments, we study the antiarrhythmic potential of late $I_{Ca,L}$ reduction at suppressing and/or preventing EAD-mediated arrhythmias in intact hearts. To test the robustness of the intervention, we use the following animal models of EAD-mediated VT/VF: (1) aged rat hearts exposed to H_2O_2 (100 µM), (2) young rat hearts exposed to hypokalemia (2 mM K^+), and (3) adult rabbit hearts exposed to hypokalemia (1 mM K^+) + H_2O_2 (100 µM). These three experimental paradigms generate VT/VF within minutes under stressing conditions that we have shown to induce stable EAD regimes in single myocytes. Notably, in these models, EAD-induced VT/VF do not terminate spontaneously unless intervened with drugs (Morita et al., 2009; Pezhouman et al., 2015).

Late $I_{Ca,L}$ reduction suppresses oxidative stress– and hypokalemia-induced VT/VF in rat hearts
Fig. 8 shows representative simultaneous recordings of bipolar electrograms from a perfused aged rat heart exposed to H_2O_2 (100 µM). Three electrode pairs were placed in (1) left atrium, (2) right ventricle, and (3) right atrium–left ventricle (p-ECG). Also, a glass microelectrode was inserted in the left ventricle to monitor the cell membrane potential during the experiment (Fig. 8 B). The microelectrode captured a series of EADs
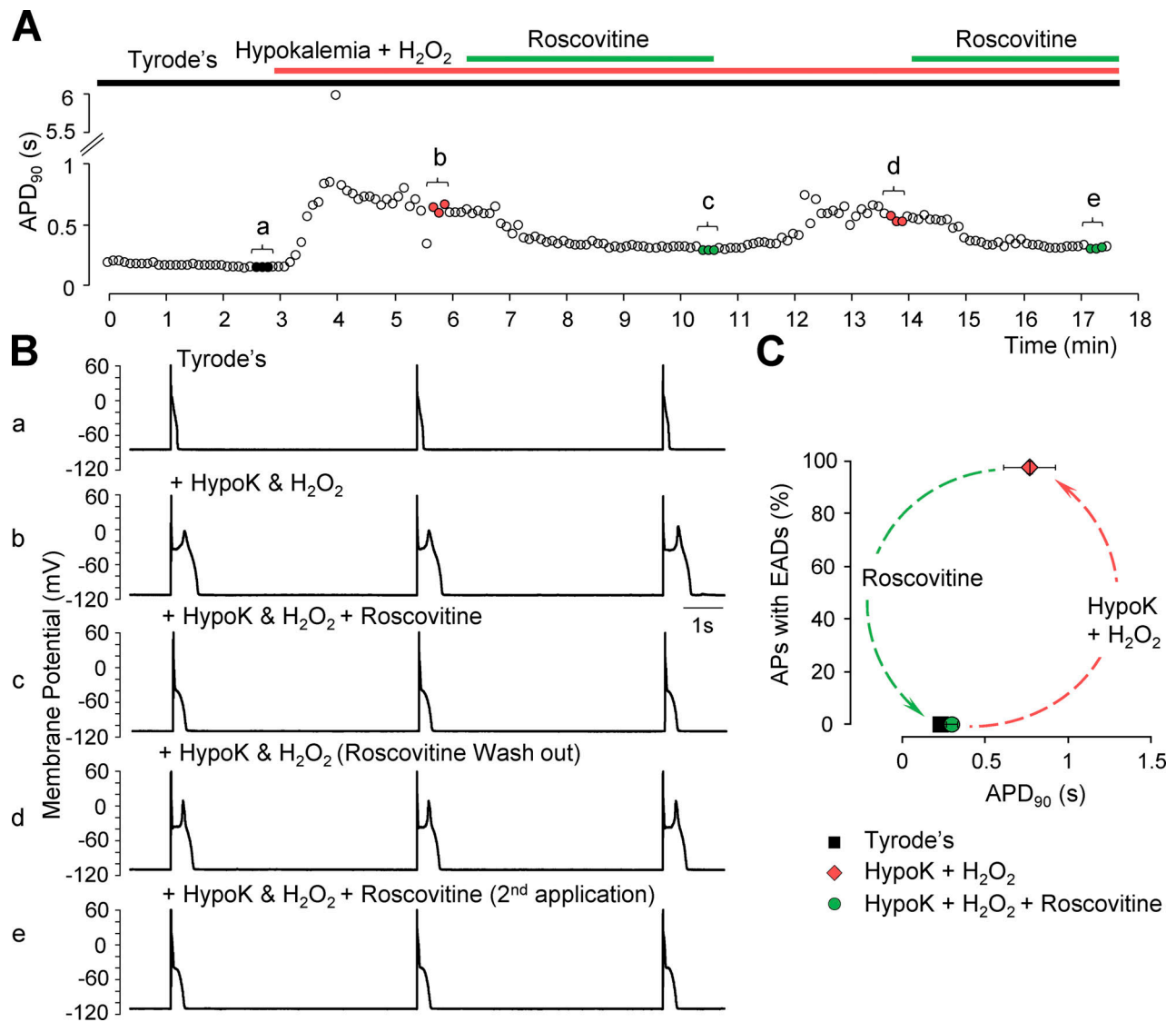
Figure 5. **Roscovitine reversibly suppresses hypokalemia and oxidative stress–induced EADs in ventricular myocytes. (A and B)** Time course of APD_{90} (A) and selected APs (B) from the same myocyte for a representative experiment testing the EAD-suppressing action of 20 µM roscovitine. A, a and B, a show AP recordings in control condition (Tyrode's solution). Hypokalemia (HypoK; 2 mM K^+) + 100 µM H_2O_2 perfusion induced a robust EAD regime (B, b), indicated by the sudden and dramatic increases of APD_{90} (A, b). Extracellular addition of roscovitine (20 µM) completely abolished EAD occurrence and restored the normal AP duration despite the continuous presence of the stressors (A, c and B, c). The acute effect of roscovitine was reversible: following a washout of the drug from the extracellular solution, the APs were prolonged and EADs reappeared within a few minutes (A, d and B, d). The EAD regime was again abolished by a second application of roscovitine (A, e and B, e). **(C)** Summary of the average changes in APD_{90} and EAD occurrence during experiments performed as in A. Note that roscovitine suppressed EADs and restored a normal APD_{90}, despite the continuous presence of stressors (n = 6, N = 5; mean ± SEM).

preceding the initiation of VT (Fig. 8 B): note that the sixth sinus beat suddenly gave rise to EAD-induced triggered activity, which then degenerated to VF. In eight out of eight hearts, the perfusion of 100 µM H_2O_2 induced VT/VF within 23.7 ± 4.3 min. Following the onset of VT/VF, the perfusion of roscovitine (20 µM) converted H_2O_2-induced VF to sinus rhythm in all aged rat hearts studied, within 13 ± 3 min (Fig. 8 C).

Following a similar experimental strategy, we probed the anti-arrhythmic efficacy of late $I_{Ca,L}$ suppression in an arrhythmia model induced by hypokalemia (2 mM K^+) in young rat hearts. We found that roscovitine (20 µM) suppressed hypokalemia-induced VT/VF in five out of six young rat hearts within 28 ± 9 min (Fig. S3).

Late $I_{Ca,L}$ reduction prevents oxidative stress– and hypokalemia-induced VT/VF in ex vivo perfused rabbit hearts

To further assess the antiarrhythmic action of late $I_{Ca,L}$ reduction in a species with ventricular AP morphology closely resembling that of the human heart, we studied the effect of roscovitine in isolated rabbit hearts. We used a new model of arrhythmia, which combines hypokalemia (1 mM K^+) with oxidative stress (100 µM H_2O_2). These stressors reliably induced EAD and VT/VF in young adult rabbits, allowing us to test the antiarrhythmic action of roscovitine in both isolated myocytes (Fig. 5) and in the whole heart. In this animal model, instead of attempting VT/VF suppression as in rat hearts, we tested the
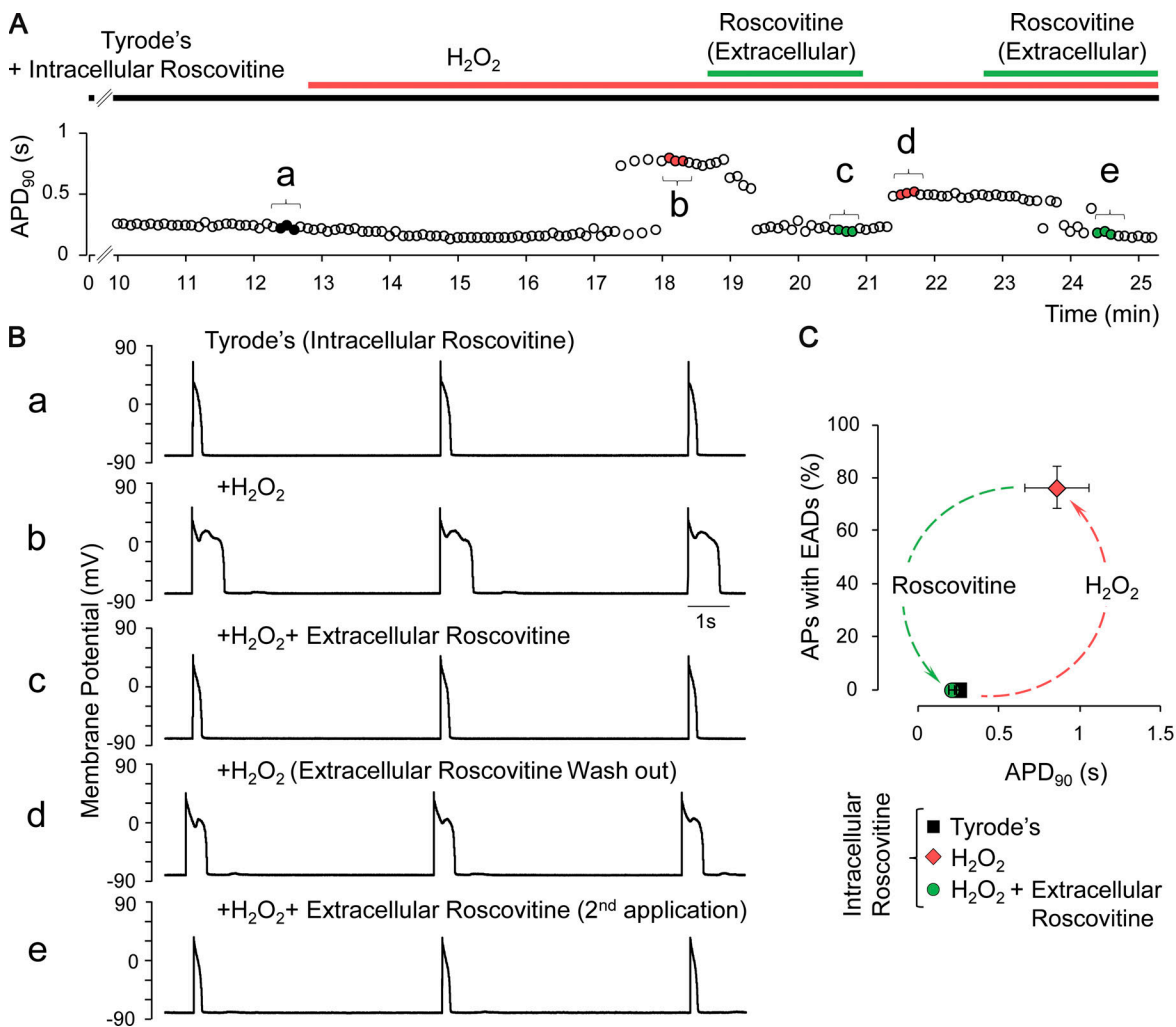
Angelini et al.
Ca$_V$1.2 gating modification as antiarrhythmic strategy

Journal of General Physiology 9 of 17
https://doi.org/10.1085/jgp.202012584

Figure 6. **EADs are not prevented by intracellular application of roscovitine and are suppressed by extracellularly applied roscovitine. (A and B)** Time course of the APD_{90} (A) and selected APs (B) from a rabbit ventricular myocyte in which 20 µM roscovitine was added to the intracellular (pipette) recording solution. A, a and B, a show AP recordings in control condition (Tyrode's solution). In spite of the presence of intracellular roscovitine, 600 µM H_2O_2 was still able to induce a robust EAD regime (A, b and B, b), which was reversibly suppressed by the application of 20 µM extracellular roscovitine (A, c and B, c). The acute effect of roscovitine was reversible: following a washout of the drug from the extracellular solution, the APs were prolonged and EADs reappeared within a minute (A, d and B, d). The EAD regime was again abolished by a second application of roscovitine (A, e and B, e). **(C)** The plot quantifies the average changes in APD_{90} and EAD incidence for experiments performed as in A ($n = 6$, $N = 4$; mean ± SEM). Note that roscovitine acted reversibly from the extracellular side of the cells to potently suppress EADs.

ability of late $I_{Ca,L}$ pharmacological reduction to prevent arrhythmia.

In the absence of roscovitine, the exposure of isolated rabbit hearts to hypokalemia + H_2O_2 induced VT/VF in five out of five rabbit hearts within 22 ± 6 min, which persisted longer than 60 min of observation (Fig. 9 B). To test whether pretreatment with roscovitine prevented VT/VF, we perfused the hearts with roscovitine for 15 min before exposure to the proarrhythmic stressors (Fig. 9 A). The pretreatment with 20 µM roscovitine prevented VT/VF during the subsequent 60 min in two out of five hearts studied (P = 0.058, log-rank test), after which the experiment was terminated (Fig. 9, C and D). Raising roscovitine concentration to 50 µM prevented VT/VF initiation in four out of five hearts (P = 0.015, log-rank test; Fig. 9, C and D).

Thus, using three models of cardiac arrhythmias in two different species, these results provide the first evidence that

selective pharmacological reduction of late $I_{Ca,L}$ suppresses and prevents EAD-mediated VT/VF induced by different stressors (hypokalemia and/or oxidative stress).

Discussion

The relevance of the $I_{Ca,L}$ window current to EAD formation was hypothesized almost three decades ago (January and Riddle, 1989), but surprisingly, no antiarrhythmic therapies based on this premise have been developed to date. In a dynamic-clamp–based study, we previously demonstrated that the selective reduction of noninactivating $I_{Ca,L}$ (late $I_{Ca,L}$), which essentially decreases the area of the $I_{Ca,L}$ window current region (Fig. 1), potently suppresses ventricular EADs (Madhvani et al., 2015). We also predicted that such a maneuver would have a minor effect on excitation–contraction coupling, thus representing an
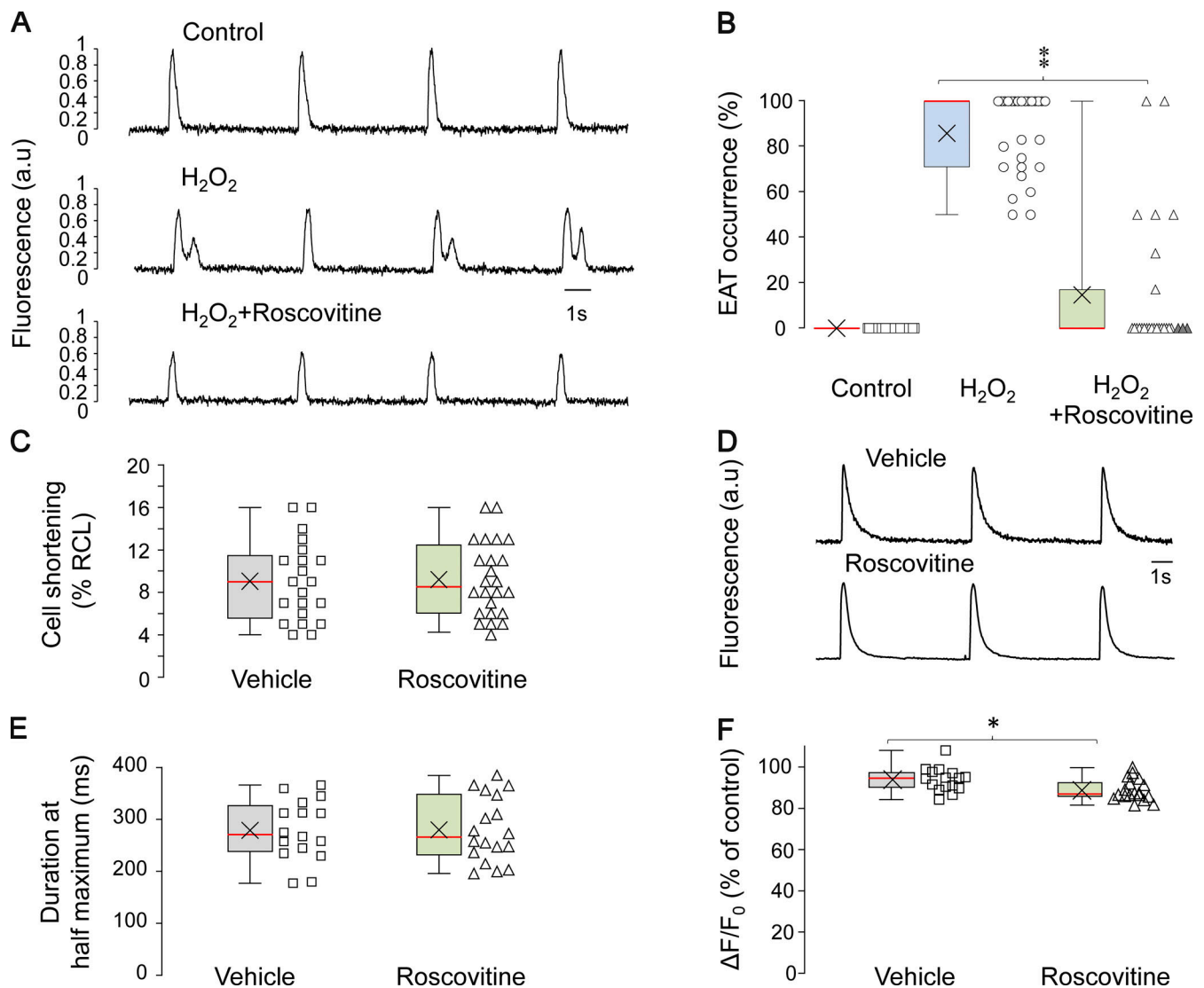
Figure 7. **Roscovitine at EAD-suppressing concentration abolishes oxidative stress–induced EATs without affecting the normal Ca²⁺ transient duration and cell shortening of ventricular myocytes. (A)** Representative Ca²⁺ transients from field-stimulated ventricular myocytes loaded with the Ca²⁺ indicator Fluo-4 AM in control (Tyrode's solution), after the addition of 200 µM H₂O₂ and in the presence of roscovitine (20 µM). Note that roscovitine suppressed EATs. **(B)** Box plot summarizing the occurrence of EATs in control, with H₂O₂, or the combination of roscovitine with H₂O₂ (n = 27, N = 8; grey triangle indicates experiments with 40 µM roscovitine; vertical asterisks, P < 0.001). **(C)** Box plot showing that cell shortening was not impaired by roscovitine (vehicle: n = 21, N = 4; roscovitine: n = 24, N = 4). **(D)** Representative Ca²⁺ transients from ventricular myocytes exposed to vehicle (0.02% DMSO) or roscovitine (20 µM). **(E)** Duration of the Ca²⁺ transient at half-maximal amplitude for vehicle (n = 16, N = 7) or roscovitine (n = 18, N = 9). **(F)** Average change in Ca²⁺ transient amplitude for vehicle (n = 16, N = 7) or roscovitine (n = 18, N = 9; *, P < 0.05). a.u, arbitrary unit. Box plots indicate first and third quartiles, median (red line), and mean (X); whiskers indicate 5 and 95 percentiles.

antiarrhythmic strategy with a significant advantage over the current class IV antiarrhythmics (LTCC blockers), which may cause adverse inotropic effects due to peak $I_{Ca,L}$ blockade (Szentandrassy et al., 2015; Godfraind, 2017). The antiarrhythmic effect associated with ventricular $I_{Ca,L}$ window current reduction has so far been supported by computational studies both at the cellular level (Madhvani et al., 2011; Madhvani et al., 2015) and more recently at the organ level, using a human anatomical ventricle model (Liu et al., 2019). However, an experimental validation of these concepts has never been pursued. The present work fills in this gap in knowledge by experimentally testing the hypothesis that drug-induced reduction of late $I_{Ca,L}$ can

effectively suppress EADs and EAD-mediated arrhythmias, providing a mechanistic link between the antiarrhythmic effect of roscovitine and its action on the $I_{Ca,L}$ window current.

We demonstrated that a selective reduction of both late $I_{Ca,L}$ and the window current region can be achieved by extracellular perfusion of roscovitine in native rabbit ventricular $I_{Ca,L}$ and in the human Ca$_V$1.2 channel (Fig. 2, Fig. 3, Fig. S1, and Fig. S2). Pharmacological reduction of late $I_{Ca,L}$ was highly effective at suppressing EADs induced by different underlying mechanisms (oxidative stress and hypokalemia) in isolated ventricular myocytes (Fig. 4, Fig. 5, and Fig. 6), experimentally confirming previous predictions (Madhvani et al., 2015; Markandeya and
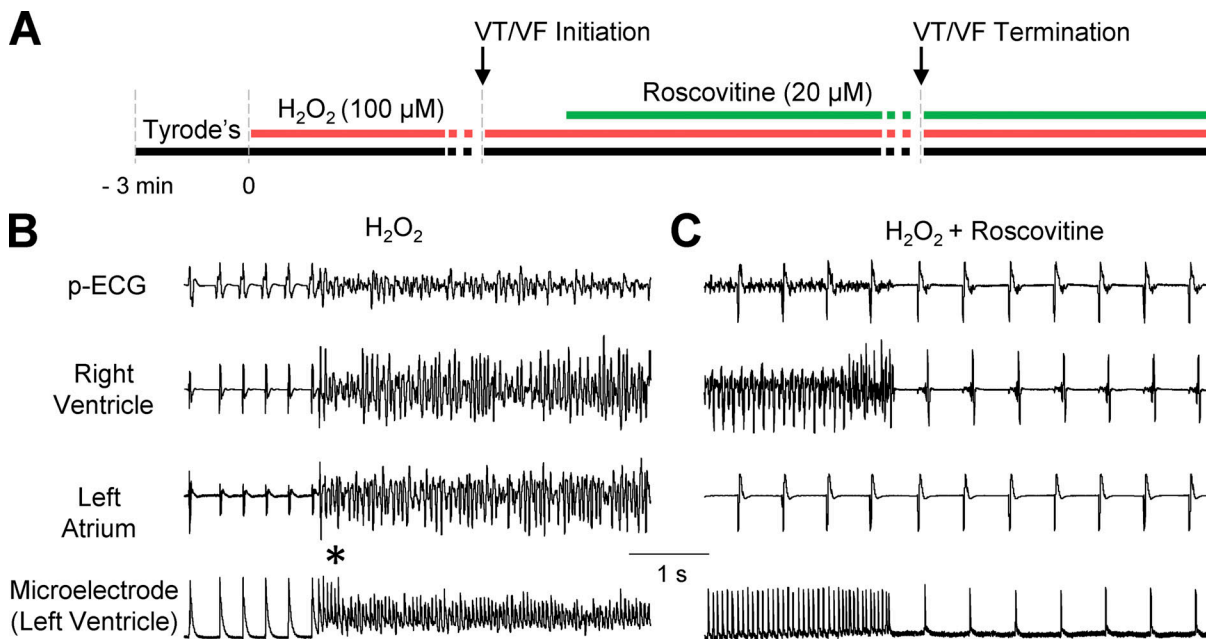
Angelini et al.
Ca$_V$1.2 gating modification as antiarrhythmic strategy

Journal of General Physiology 11 of 17
https://doi.org/10.1085/jgp.202012584

Figure 8. **Roscovitine terminates VT/VF in aged rat hearts. (A)** Experimental protocol used to test the ability of roscovitine to suppress VT/VF in ex vivo perfused aged rat hearts. **(B and C)** Bipolar electrograms and microelectrode recordings from the indicated chambers of the heart. p-ECGs were obtained from right atrial–left ventricular leads. Single-cell APs were measured by a glass microelectrode inserted in the left ventricle epicardium. **(B)** The recordings show initiation of VF, which occurred 38 min after exposure to 100 µM H$_2$O$_2$. Note the initiation of VF by cellular EAD-mediated triggered activity, which arose suddenly during sinus rhythm (microelectrode, *). **(C)** Recordings from the same heart as in B, showing suppression of VF 16 min after the addition of ro-scovitine (20 µM) to the perfusate, in the continuous presence of H$_2$O$_2$.

Kamp, 2015). In addition to I$_{Ca,L}$, the Na$^+$/Ca^{2+} exchanger has also been shown to contribute to EAD formation (Szabo et al., 1994; Wit, 2018). Therefore, it is conceivable that a reduction of the late I$_{Ca,L}$ could also decrease Na$^+$/Ca^{2+} exchanger activity during the AP, contributing to the beneficial suppression of EADs. Furthermore, our findings establish that the cellular effects of roscovitine translate to the whole organ level, where it potently suppresses and prevents EAD-mediated VT/VF in isolated per-fused hearts of two species with different AP characteristics (rabbit and rat; Fig. 8, Fig. 9, and Fig. S3). Since roscovitine largely preserves Ca^{2+} transient amplitude and duration and myocyte shortening (Fig. 7, C–F), we expect that heart contrac-tility will be minimally, if at all, affected. Consistent with these findings, the application of roscovitine in induced pluripotent stem cell–derived cardiomyocytes from patients with Timothy syndrome (LQT8) was found to restore normal electrical activity and Ca^{2+} handling at the single-cell level (Yazawa et al., 2011; Song et al., 2015; Song et al., 2017).

The efficacy and safety of this strategy in comparison with LTCC blockade (class IV antiarrhythmics) is illustrated in Fig. S4. Specifically, we simulated I$_{Ca,L}$ in a virtual myocyte exposed to oxidative stress and exhibiting EADs, as well as in a cell under normal conditions exhibiting normal APs. Under oxidative stress conditions, LTCCs with a reduced noninactivating com-ponent (i.e., with reduced late I$_{Ca,L}$; Fig. S4 A) conduct less current during late phases of the AP, when EADs occur (Fig. S4 B). Accordingly, were this a real cell (myocyte), the reduced inward current would likely facilitate AP repolarization and suppression of the EAD regime, as was shown in dynamic-clamp

experiments (Madhvani et al., 2015) and the pharmacological reduction of the late I$_{Ca,L}$ (this work). Note that late I$_{Ca,L}$ re-duction did not affect the early component of I$_{Ca,L}$ under oxi-dative stress conditions (Fig. S4 B) or the whole I$_{Ca,L}$ during normal conditions (Fig. S4 C). These results offer an explanation as to why Ca^{2+} transients and myocyte contractility were largely preserved during roscovitine application (Fig. 7, C–F). In con-trast, a simulated 20% LTCC blockade (Fig. S4 D) resulted in reduced I$_{Ca,L}$ during all AP phases in both oxidative stress (Fig. S4 E) and normal (Fig. S4 F) conditions, consistent with the action of LTCC blockers (class IV antiarrhythmics), which may potently abolish arrhythmias at the expense of compromised contractility (reduced early I$_{Ca,L}$; Markandeya and Kamp, 2015; Godfraind, 2017; Karagueuzian et al., 2017).

The roscovitine site of antiarrhythmic action
Our results have provided evidence for an extracellular action of roscovitine on Ca$_V$1.2, which reduces late I$_{Ca,L}$ and, in turn, suppresses EAD-sustained arrhythmias. Roscovitine has been reported to also inhibit intracellular cyclin-dependent kinases (CDKs; Meijer et al., 1997; Bach et al., 2005; Sánchez-Martínez et al., 2015; Song et al., 2017) and other kinases including CaMKII (Meijer et al., 1997; Bach et al., 2005; Sánchez-Martínez et al., 2015). While it is possible that some of the effects on LTCCs are mediated by intracellular effectors (e.g., CaMKII), our data from isolated myocytes show that (1) intracellular application of 20 µM roscovitine did not prevent or suppress EADs (Fig. 6) and (2) the suppression of EADs by roscovitine could be rapidly re-versed by washing out the drug (Fig. 5 and Fig. 6). Together, this
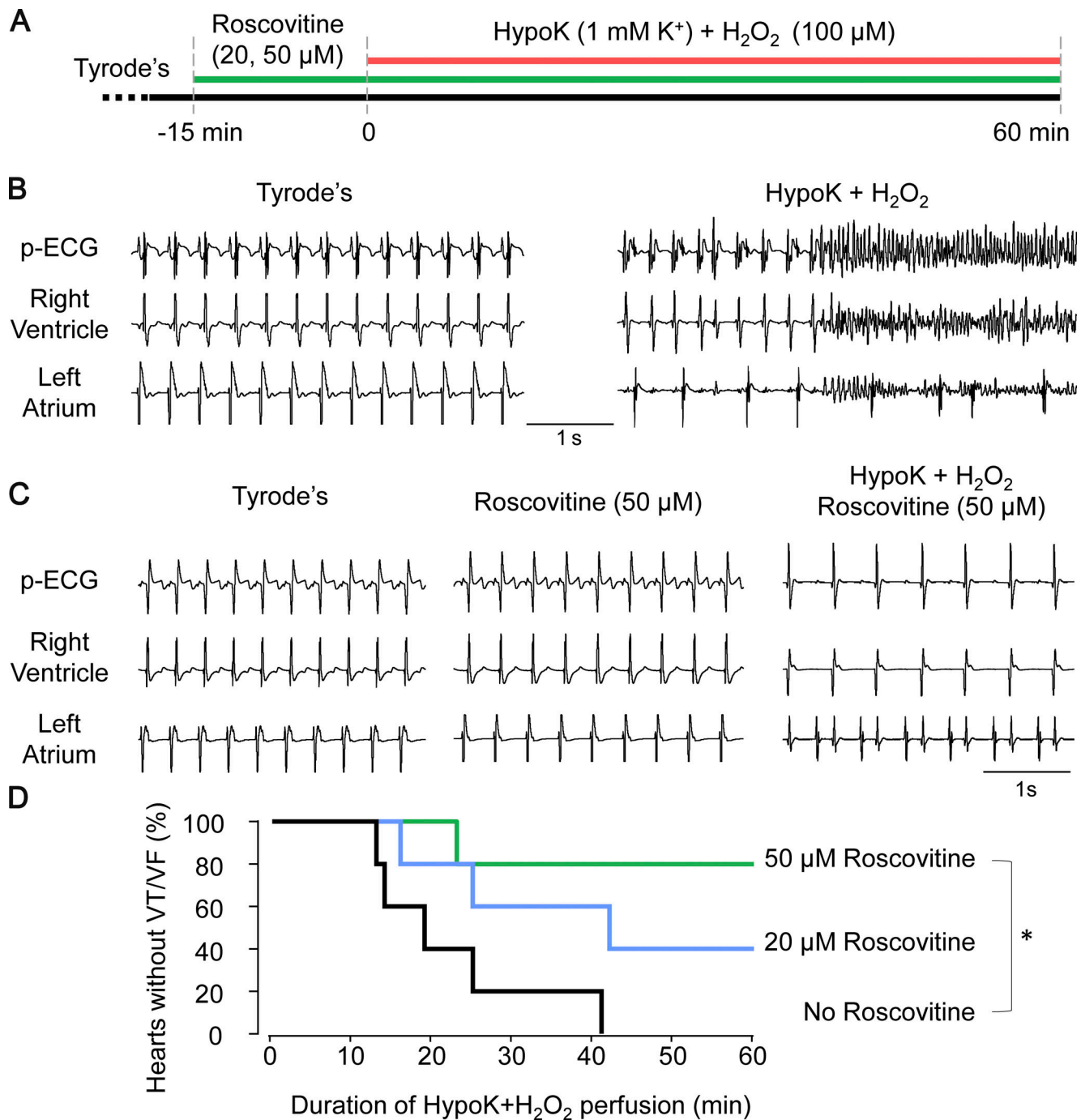
Figure 9. **Roscovitine prevents the induction of VT/VF by hypokalemia and oxidative stress in ex vivo rabbit hearts. (A)** Experimental protocol used to test the ability of roscovitine to prevent VT/VF in ex vivo perfused aged rabbit hearts. **(B)** Bipolar electrograms from the indicated chambers of the heart. p-ECGs were obtained from right atrial–left ventricular leads. Left panel shows a representative experiment in control condition (Tyrode's solution). Right panel shows the initiation of VT/VF in the same heart 14 min after perfusion of a hypokalemic (HypoK; 1 mM K$^+$) Tyrode's containing 100 µM H$_2$O$_2$. **(C)** Representative bipolar electrograms in control condition (left), after 15-min pretreatment with 50 µM roscovitine (middle), and 60 min after the perfusion of hypokalemia + 100 µM H$_2$O$_2$ in the presence of roscovitine (right). Note that roscovitine prevented the initiation of VT/VF. **(D)** Kaplan–Meier plot comparing time to onset of VT/VF for hearts exposed to hypokalemia and H$_2$O$_2$ in control (black) or in the presence of 20 or 50 µM roscovitine (n = 5 hearts per condition; *, $P < 0.05$).

evidence suggests that possible kinase inhibition by roscovitine is not sufficient to account for its EAD-suppressing effects. These findings are in agreement with a previous study that found that intracellular application of 300 µM roscovitine did not modify LTCC gating properties, prompting the authors to suggest that the roscovitine-induced modification of Ca$_V$1.2 channels is not mediated by a kinase-dependent mechanism (Yarotskyy and Elmslie, 2007). In a chimera-based study, an

Angelini et al.
Ca$_V$1.2 gating modification as antiarrhythmic strategy

Journal of General Physiology 13 of 17
https://doi.org/10.1085/jgp.202012584

extracellular roscovitine binding site responsible for enhanced LTCC inactivation (i.e., late $I_{Ca,L}$ reduction) has been located in the Repeat I of the $Ca_V1.2$ pore-forming subunit (Yarotskyy et al., 2010).

Roscovitine has been shown to block other cardiac ion channels. Heterologously expressed hERG channels were inhibited by roscovitine with a half-maximal inhibitory concentration (IC_{50}) of 27 μM in HEK cells and an IC_{50} of ~200 μM in oocytes (Ganapathi et al., 2009; Cernuda et al., 2019). $K_V4.2$ voltage-dependent potassium channels have also been shown to be sensitive to roscovitine (Buraei et al., 2007). Block of potassium channels is more likely to promote (rather than suppress) EAD-mediated arrhythmias by further reducing repolarization reserve and increasing AP duration (Sanguinetti and Tristani-Firouzi, 2006; Roden, 2016; Weiss et al., 2017). This suggests that the antiarrhythmic properties of roscovitine are largely due to its action on the LTCC. Notably, in clinical trials assessing its anti-cancer potential, roscovitine was well tolerated, and no instances of cardiac proarrhythmia or other cardiac side effects were reported (Fischer and Gianella-Borradori, 2003; Benson et al., 2007).

LTCC blockers versus gating modifiers: A new class of antiarrhythmics?

Currently, class IV antiarrhythmics, such as diltiazem and verapamil, are in clinical use for the treatment and prevention of various cardiac arrhythmias (Rosen et al., 1975; Grace and Camm, 2000; Szentandrassy et al., 2015; Godfraind, 2017). The primary action of these drugs is to block LTCC conductance, indiscriminately reducing both late and peak $I_{Ca,L}$ (Fig. S4, D–F). While suppressing EADs (January et al., 1988; Shimizu et al., 1995; Hensley et al., 1997), the overall suppression of Ca^{2+} influx causes an adverse, negative-inotropic effect that limits their therapeutic value, especially in patients with compromised cardiac function (Rosen et al., 1975; Russell, 1988; Elliott and Ram, 2011). Importantly, while suppression of peak $I_{Ca,L}$ is not safe, it is also not necessary to suppress EAD-mediated arrhythmias. We propose that drugs selectively reducing late $I_{Ca,L}$, or the LTCC window current, constitute a new class of antiarrhythmic drug action. Roscovitine, which selectively blocks late $I_{Ca,L}$, represents a prototypical member of this class (Karagueuzian et al., 2017).

Indeed, the structural similarities of Na_V and Ca_V channels (Catterall and Swanson, 2015) and the development and clinical use of therapeutic compounds targeting late Na^+ current (GS-967, eleclazine, ranolazine; Antzelevitch et al., 2004; Belardinelli et al., 2013; Sicouri et al., 2013; Pezhouman et al., 2014; Fuller et al., 2016; Bengel et al., 2017; Bossu et al., 2018; Hwang et al., 2020; Reed et al., 2021) support the feasibility of developing drugs that selectively reduce late $I_{Ca,L}$.

In conclusion, we believe that the results of the present study set the framework for the development of a conceptually new class of antiarrhythmics (LTCC gating modifiers) that selectively reduce late $I_{Ca,L}$ and suppress EAD-mediated arrhythmias. More generally, these results raise the exciting possibility that ion channel gating modification, without ion channel blockade, holds promise for the design of next-generation antiarrhythmics (Antzelevitch et al., 2004; Belardinelli et al., 2013; Pezhouman

et al., 2014; Liin et al., 2015; Bengel et al., 2017; Bossu et al., 2018; Larsson et al., 2018; Salari et al., 2018).

Study limitations

Roscovitine is a purine-based compound that has been used in clinical trials for its anti-cancer action and displays a broad spectrum of effects. In its native form, its CDK-inhibiting activity might preclude its clinical use as an antiarrhythmic. However, we are encouraged that (1) the Ca^{2+} channel gating modification is extracellular, whereas the CDK effects are intracellular (Sánchez-Martínez et al., 2015), and (2) roscovitine analogues with reduced CDK inhibition are already known, raising the possibility that the Ca^{2+} channel and CDK effects could be separated in novel derivative compounds (Liang et al., 2012; Wu et al., 2018), providing effective antiarrhythmic action.

References

Antoons, G., P.G. Volders, T. Stankovicova, V. Bito, M. Stengl, M.A. Vos, and K.R. Sipido. 2007. Window Ca^{2+} current and its modulation by Ca^{2+} release in hypertrophied cardiac myocytes from dogs with chronic atrioventricular block. *J. Physiol.* 579:147–160. https://doi.org/10.1113/jphysiol.2006.124222

Antzelevitch, C., and A. Burashnikov. 2011. Overview of basic mechanisms of cardiac arrhythmia. *Card. Electrophysiol. Clin.* 3:23–45. https://doi.org/10.1016/j.ccep.2010.10.012

Antzelevitch, C., L. Belardinelli, A.C. Zygmunt, A. Burashnikov, J.M. Di Diego, J.M. Fish, J.M. Cordeiro, and G. Thomas. 2004. Electrophysiological

effects of ranolazine, a novel antianginal agent with antiarrhythmic properties. *Circulation.* 110:904–910. https://doi.org/10.1161/01.CIR.0000139333.83620.5D

Bach, S., M. Knockaert, J. Reinhardt, O. Lozach, S. Schmitt, B. Baratte, M. Koken, S.P. Coburn, L. Tang, T. Jiang, et al. 2005. Roscovitine targets, protein kinases and pyridoxal kinase. *J. Biol. Chem.* 280:31208–31219. https://doi.org/10.1074/jbc.M500806200

Banyasz, T., N. Szentandrássy, J. Magyar, Z. Szabo, P.P. Nánási, Y. Chen-Izu, and L.T. Izu. 2015. An emerging antiarrhythmic target: late sodium current. *Curr. Pharm. Des.* 21:1073–1090. https://doi.org/10.2174/1381612820666141029111729

Bapat, A., T.P. Nguyen, J.H. Lee, A.A. Sovari, M.C. Fishbein, J.N. Weiss, and H.S. Karagueuzian. 2012. Enhanced sensitivity of aged fibrotic hearts to angiotensin II- and hypokalemia-induced early afterdepolarization-mediated ventricular arrhythmias. *Am. J. Physiol. Heart Circ. Physiol.* 302:H2331–H2340. https://doi.org/10.1152/ajpheart.00094.2012

Barish, M.E. 1983. A transient calcium-dependent chloride current in the immature *Xenopus* oocyte. *J. Physiol.* 342:309–325. https://doi.org/10.1113/jphysiol.1983.sp014852

Belardinelli, L., G. Liu, C. Smith-Maxwell, W.Q. Wang, N. El-Bizri, R. Hirakawa, S. Karpinski, C.H. Li, L. Hu, X.J. Li, et al. 2013. A novel, potent, and selective inhibitor of cardiac late sodium current suppresses experimental arrhythmias. *J. Pharmacol. Exp. Ther.* 344:23–32. https://doi.org/10.1124/jpet.112.198887

Bengel, P., S. Ahmad, and S. Sossalla. 2017. Inhibition of late sodium current as an innovative antiarrhythmic strategy. *Curr. Heart Fail. Rep.* 14:179–186. https://doi.org/10.1007/s11897-017-0333-0

Benjamin, E.J., S.S. Virani, C.W. Callaway, A.M. Chamberlain, A.R. Chang, S. Cheng, S.E. Chiuve, M. Cushman, F.N. Delling, R. Deo, et al. American Heart Association Council on Epidemiology and Prevention Statistics Committee and Stroke Statistics Subcommittee. 2018. Heart Disease and Stroke Statistics-2018 Update: A Report From the American Heart Association. *Circulation.* 137:e67–e492. https://doi.org/10.1161/CIR.0000000000000558

Benson, C., J. White, J. De Bono, A. O'Donnell, F. Raynaud, C. Cruickshank, H. McGrath, M. Walton, P. Workman, S. Kaye, et al. 2007. A phase I trial of the selective oral cyclin-dependent kinase inhibitor seliciclib (CYC202; R-Roscovitine), administered twice daily for 7 days every 21 days. *Br. J. Cancer.* 96:29–37. https://doi.org/10.1038/sj.bjc.6603509

Bers, D.M. 2002. Cardiac excitation-contraction coupling. *Nature.* 415:198–205. https://doi.org/10.1038/415198a

Bossu, A., M.J.C. Houtman, V.M.F. Meijborg, R. Varkevisser, H.D.M. Beekman, A. Dunnink, J.M.T. de Bakker, N. Mollova, S. Rajamani, L. Belardinelli, et al. 2018. Selective late sodium current inhibitor GS-458967 suppresses Torsades de Pointes by mostly affecting perpetuation but not initiation of the arrhythmia. *Br. J. Pharmacol.* 175:2470–2482. https://doi.org/10.1111/bph.14217

Brehm, P., and R. Eckert. 1978. Calcium entry leads to inactivation of calcium channel in Paramecium. *Science.* 202:1203–1206. https://doi.org/10.1126/science.103199

Buraei, Z., G. Schofield, and K.S. Elmslie. 2007. Roscovitine differentially affects CaV2 and Kv channels by binding to the open state. *Neuropharmacology.* 52:883–894. https://doi.org/10.1016/j.neuropharm.2006.10.006

Catterall, W.A., and T.M. Swanson. 2015. Structural basis for pharmacology of voltage-gated sodium and calcium channels. *Mol. Pharmacol.* 88:141–150. https://doi.org/10.1124/mol.114.097659

Cernuda, B., C.T. Fernandes, S.M. Allam, M. Orzillo, G. Suppa, Z. Chia Chang, D. Athanasopoulos, and Z. Buraei. 2019. The molecular determinants of R-roscovitine block of hERG channels. *PLoS One.* 14:e0217733. https://doi.org/10.1371/journal.pone.0217733

Chen-Izu, Y., R.M. Shaw, G.S. Pitt, V. Yarov-Yarovoy, J.T. Sack, H. Abriel, R.W. Aldrich, L. Belardinelli, M.B. Cannell, W.A. Catterall, et al. 2015. Na$^+$ channel function, regulation, structure, trafficking and sequestration. *J. Physiol.* 593:1347–1360. https://doi.org/10.1113/jphysiol.2014.281428

Chugh, S.S., K. Reinier, C. Teodorescu, A. Evanado, E. Kehr, M. Al Samara, R. Mariani, K. Gunson, and J. Jui. 2008. Epidemiology of sudden cardiac death: clinical and research implications. *Prog. Cardiovasc. Dis.* 51:213–228. https://doi.org/10.1016/j.pcad.2008.06.003

Cranefield, P.F., and R.S. Aronson. 1991. Torsades de pointes and early afterdepolarizations. *Cardiovasc. Drugs Ther.* 5:531–537. https://doi.org/10.1007/BF03029780

Cygankiewicz, I. 2020. Sudden cardiac death—epidemiology and demographics. *In* Sex and Cardiac Electrophysiology. M. Malik, editor.

Academic Press, London. 739–745. https://doi.org/10.1016/B978-0-12-817728-0.00066-8

Eisner, D.A., W.J. Lederer, and C. Ojeda. 1978. Arrhythmogenic effects of hypokalaemia on mammalian ventricular muscle [proceedings]. *J. Physiol.* 280:74P–75P.

Eisner, D.A., J.L. Caldwell, K. Kistamás, and A.W. Trafford. 2017. Calcium and excitation-contraction coupling in the heart. *Circ. Res.* 121:181–195. https://doi.org/10.1161/CIRCRESAHA.117.310230

Elliott, W.J., and C.V. Ram. 2011. Calcium channel blockers. *J. Clin. Hypertens. (Greenwich).* 13:687–689. https://doi.org/10.1111/j.1751-7176.2011.00513.x

Fischer, P.M., and A. Gianella-Borradori. 2003. CDK inhibitors in clinical development for the treatment of cancer. *Expert Opin. Investig. Drugs.* 12:955–970. https://doi.org/10.1517/13543784.12.6.955

Fuller, H., F. Justo, B.D. Nearing, K.M. Kahlig, S. Rajamani, L. Belardinelli, and R.L. Verrier. 2016. Eleclazine, a new selective cardiac late sodium current inhibitor, confers concurrent protection against autonomically induced atrial premature beats, repolarization alternans and heterogeneity, and atrial fibrillation in an intact porcine model. *Heart Rhythm.* 13:1679–1686. https://doi.org/10.1016/j.hrthm.2016.04.015

Ganapathi, S.B., M. Kester, and K.S. Elmslie. 2009. State-dependent block of HERG potassium channels by R-roscovitine: implications for cancer therapy. *Am. J. Physiol. Cell Physiol.* 296:C701–C710. https://doi.org/10.1152/ajpcell.00633.2008

George, A.L. Jr. 2013. Molecular and genetic basis of sudden cardiac death. *J. Clin. Invest.* 123:75–83. https://doi.org/10.1172/JCI62928

Godfraind, T. 2017. Discovery and development of calcium channel blockers. *Front. Pharmacol.* 8:286. https://doi.org/10.3389/fphar.2017.00286

Goldhaber, J.I., and E. Liu. 1994. Excitation-contraction coupling in single guinea-pig ventricular myocytes exposed to hydrogen peroxide. *J. Physiol.* 477:135–147. https://doi.org/10.1113/jphysiol.1994.sp020178

Grace, A.A., and A.J. Camm. 2000. Voltage-gated calcium-channels and antiarrhythmic drug action. *Cardiovasc. Res.* 45:43–51. https://doi.org/10.1016/S0008-6363(99)00306-5

Greensmith, D.J., D.A. Eisner, and M. Nirmalan. 2010. The effects of hydrogen peroxide on intracellular calcium handling and contractility in the rat ventricular myocyte. *Cell Calcium.* 48:341–351. https://doi.org/10.1016/j.ceca.2010.10.007

Hensley, J., G.E. Billman, J.D. Johnson, C.M. Hohl, and R.A. Altschuld. 1997. Effects of calcium channel antagonists on Ca^{2+} transients in rat and canine cardiomyocytes. *J. Mol. Cell. Cardiol.* 29:1037–1043. https://doi.org/10.1006/jmcc.1996.0348

Hullin, R., I.F. Khan, S. Wirtz, P. Mohacsi, G. Varadi, A. Schwartz, and S. Herzig. 2003. Cardiac L-type calcium channel beta-subunits expressed in human heart have differential effects on single channel characteristics. *J. Biol. Chem.* 278:21623–21630. https://doi.org/10.1074/jbc.M211164200

Hwang, J., T.Y. Kim, D. Terentyev, M. Zhong, A.Y. Kabakov, P. Bronk, K. Arunachalam, L. Belardinelli, S. Rajamani, Y. Kunitomo, et al. 2020. Late I$_{Na}$ Blocker GS967 Supresses Polymorphic Ventricular Tachycardia in a Transgenic Rabbit Model of Long QT Type 2. *Circ. Arrhythm. Electrophysiol.* 13:e006875. https://doi.org/10.1161/CIRCEP.118.006875

January, C.T., and J.M. Riddle. 1989. Early afterdepolarizations: mechanism of induction and block. A role for L-type Ca^{2+} current. *Circ. Res.* 64:977–990. https://doi.org/10.1161/01.RES.64.5.977

January, C.T., J.M. Riddle, and J.J. Salata. 1988. A model for early afterdepolarizations: induction with the Ca^{2+} channel agonist Bay K 8644. *Circ. Res.* 62:563–571. https://doi.org/10.1161/01.RES.62.3.563

Karagueuzian, H.S., T.P. Nguyen, Z. Qu, and J.N. Weiss. 2013. Oxidative stress, fibrosis, and early afterdepolarization-mediated cardiac arrhythmias. *Front. Physiol.* 4:19. https://doi.org/10.3389/fphys.2013.00019

Karagueuzian, H.S., A. Pezhouman, M. Angelini, and R. Olcese. 2017. Enhanced late Na and Ca currents as effective antiarrhythmic drug targets. *Front. Pharmacol.* 8:36. https://doi.org/10.3389/fphar.2017.00036

Kass, R.S., and M.C. Sanguinetti. 1984. Inactivation of calcium channel current in the calf cardiac Purkinje fiber. Evidence for voltage- and calcium-mediated mechanisms. *J. Gen. Physiol.* 84:705–726. https://doi.org/10.1085/jgp.84.5.705

Kettlewell, S., P. Saxena, J. Dempster, M.A. Colman, R.C. Myles, G.L. Smith, and A.J. Workman. 2019. Dynamic clamping human and rabbit atrial calcium current: narrowing I$_{CaL}$ window abolishes early afterdepolarizations. *J. Physiol.* 597:3619–3638. https://doi.org/10.1113/JP277827

Kimrey, J., T. Vo, and R. Bertram. 2020. Canard analysis reveals why a large Ca^{2+} window current promotes early afterdepolarizations in cardiac

myocytes. *PLOS Comput. Biol.* 16:e1008341. https://doi.org/10.1371/journal.pcbi.1008341

Kong, M.H., G.C. Fonarow, E.D. Peterson, A.B. Curtis, A.F. Hernandez, G.D. Sanders, K.L. Thomas, D.L. Hayes, and S.M. Al-Khatib. 2011. Systematic review of the incidence of sudden cardiac death in the United States. *J. Am. Coll. Cardiol.* 57:794–801. https://doi.org/10.1016/j.jacc.2010.09.064

Larsson, J.E., H.P. Larsson, and S.I. Liin. 2018. KCNE1 tunes the sensitivity of $K_V7.1$ to polyunsaturated fatty acids by moving turret residues close to the binding site. *eLife.* 7:e37257. https://doi.org/10.7554/eLife.37257

Lee, K.S., E. Marban, and R.W. Tsien. 1985. Inactivation of calcium channels in mammalian heart cells: joint dependence on membrane potential and intracellular calcium. *J. Physiol.* 364:395–411. https://doi.org/10.1113/jphysiol.1985.sp015752

Li, W., Y.P. Wang, L. Gao, P.P. Zhang, Q. Zhou, Q.F. Xu, Z.W. Zhou, K. Guo, R.H. Chen, H.T. Yang, and Y.G. Li. 2013. Resveratrol protects rabbit ventricular myocytes against oxidative stress-induced arrhythmogenic activity and Ca^{2+} overload. *Acta Pharmacol. Sin.* 34:1164–1173. https://doi.org/10.1038/aps.2013.82

Liang, M., T.B. Tarr, K. Bravo-Altamirano, G. Valdomir, G. Rensch, L. Swanson, N.R. DeStefino, C.M. Mazzarisi, R.A. Olszewski, G.M. Wilson, et al. 2012. Synthesis and biological evaluation of a selective N- and p/q-type calcium channel agonist. *ACS Med. Chem. Lett.* 3:985–990. https://doi.org/10.1021/ml3002083

Liin, S.I., M. Silverå Ejneby, R. Barro-Soria, M.A. Skarsfeldt, J.E. Larsson, F. Starck Härlin, T. Parkkari, B.H. Bentzen, N. Schmitt, H.P. Larsson, and F. Elinder. 2015. Polyunsaturated fatty acid analogs act antiarrhythmically on the cardiac IKs channel. *Proc. Natl. Acad. Sci. USA.* 112:5714–5719. https://doi.org/10.1073/pnas.1503488112

Liu, M.B., N. Vandersickel, A.V. Panfilov, and Z. Qu. 2019. R-From-T as a common mechanism of arrhythmia initiation in long QT syndromes. *Circ. Arrhythm. Electrophysiol.* 12:e007571. https://doi.org/10.1161/CIRCEP.119.007571

Madhvani, R.V., Y. Xie, A. Pantazis, A. Garfinkel, Z. Qu, J.N. Weiss, and R. Olcese. 2011. Shaping a new Ca^{2+} conductance to suppress early afterdepolarizations in cardiac myocytes. *J. Physiol.* 589:6081–6092. https://doi.org/10.1113/jphysiol.2011.219600

Madhvani, R.V., M. Angelini, Y. Xie, A. Pantazis, S. Suriany, N.P. Borgstrom, A. Garfinkel, Z. Qu, J.N. Weiss, and R. Olcese. 2015. Targeting the late component of the cardiac L-type Ca^{2+} current to suppress early afterdepolarizations. *J. Gen. Physiol.* 145:395–404. https://doi.org/10.1085/jgp.201411288

Mahajan, A., Y. Shiferaw, D. Sato, A. Baher, R. Olcese, L.H. Xie, M.J. Yang, P.S. Chen, J.G. Restrepo, A. Karma, et al. 2008. A rabbit ventricular action potential model replicating cardiac dynamics at rapid heart rates. *Biophys. J.* 94:392–410. https://doi.org/10.1529/biophysj.106.98160

Maltsev, V.A., H.N. Sabbah, R.S. Higgins, N. Silverman, M. Lesch, and A.I. Undrovinas. 1998. Novel, ultraslow inactivating sodium current in human ventricular cardiomyocytes. *Circulation.* 98:2545–2552. https://doi.org/10.1161/01.CIR.98.23.2545

Markandeya, Y.S., and T.J. Kamp. 2015. Rational strategy to stop arrhythmias: Early afterdepolarizations and L-type Ca^{2+} current. *J. Gen. Physiol.* 145:475–479. https://doi.org/10.1085/jgp.201511429

Meijer, L., A. Borgne, O. Mulner, J.P. Chong, J.J. Blow, N. Inagaki, M. Inagaki, J.G. Delcros, and J.P. Moulinoux. 1997. Biochemical and cellular effects of roscovitine, a potent and selective inhibitor of the cyclin-dependent kinases cdc2, cdk2 and cdk5. *Eur. J. Biochem.* 243:527–536. https://doi.org/10.1111/j.1432-1033.1997.t01-2-00527.x

Morita, N., A.A. Sovari, Y. Xie, M.C. Fishbein, W.J. Mandel, A. Garfinkel, S.F. Lin, P.S. Chen, L.H. Xie, F. Chen, et al. 2009. Increased susceptibility of aged hearts to ventricular fibrillation during oxidative stress. *Am. J. Physiol. Heart Circ. Physiol.* 297:H1594–H1605. https://doi.org/10.1152/ajpheart.00579.2009

Morita, N., J.H. Lee, A. Bapat, M.C. Fishbein, W.J. Mandel, P.S. Chen, J.N. Weiss, and H.S. Karagueuzian. 2011a. Glycolytic inhibition causes spontaneous ventricular fibrillation in aged hearts. *Am. J. Physiol. Heart Circ. Physiol.* 301:H180–H191. https://doi.org/10.1152/ajpheart.00128.2011

Morita, N., J.H. Lee, Y. Xie, A. Sovari, Z. Qu, J.N. Weiss, and H.S. Karagueuzian. 2011b. Suppression of re-entrant and multifocal ventricular fibrillation by the late sodium current blocker ranolazine. *J. Am. Coll. Cardiol.* 57:366–375. https://doi.org/10.1016/j.jacc.2010.07.045

Morotti, S., E. Grandi, A. Summa, K.S. Ginsburg, and D.M. Bers. 2012. Theoretical study of L-type Ca^{2+} current inactivation kinetics during action potential repolarization and early afterdepolarizations. *J. Physiol.* 590:4465–4481. https://doi.org/10.1113/jphysiol.2012.231886

Neely, A., R. Olcese, X. Wei, L. Birnbaumer, and E. Stefani. 1994. $Ca^{(2+)}$-dependent inactivation of a cloned cardiac Ca^{2+} channel α_1 subunit (α_{1C}) expressed in *Xenopus* oocytes. *Biophys. J.* 66:1895–1903. https://doi.org/10.1016/S0006-3495(94)80983-X

Nguyen, T.P., Z. Qu, and J.N. Weiss. 2014. Cardiac fibrosis and arrhythmogenesis: the road to repair is paved with perils. *J. Mol. Cell. Cardiol.* 70:83–91. https://doi.org/10.1016/j.yjmcc.2013.10.018

Nguyen, T.P., N. Singh, Y. Xie, Z. Qu, and J.N. Weiss. 2015. Repolarization reserve evolves dynamically during the cardiac action potential: effects of transient outward currents on early afterdepolarizations. *Circ. Arrhythm. Electrophysiol.* 8:694–702. https://doi.org/10.1161/CIRCEP.114.002451

Osadchii, O.E. 2010. Mechanisms of hypokalemia-induced ventricular arrhythmogenicity. *Fundam. Clin. Pharmacol.* 24:547–559. https://doi.org/10.1111/j.1472-8206.2010.00835.x

Pantazis, A., and R. Olcese. 2019. Cut-Open Oocyte Voltage-Clamp Technique. *In* Encyclopedia of Biophysics. G. Roberts, and A. Watts, editors. Springer Berlin Heidelberg, Berlin, Heidelberg. https://doi.org/10.1007/978-3-642-35943-9_371-1

Peterson, B.Z., C.D. DeMaria, J.P. Adelman, and D.T. Yue. 1999. Calmodulin is the Ca^{2+} sensor for Ca^{2+}-dependent inactivation of L-type calcium channels. *Neuron.* 22:549–558. https://doi.org/10.1016/S0896-6273(00)80709-6

Pezhouman, A., S. Madahian, H. Stepanyan, H. Ghukasyan, Z. Qu, L. Belardinelli, and H.S. Karagueuzian. 2014. Selective inhibition of late sodium current suppresses ventricular tachycardia and fibrillation in intact rat hearts. *Heart Rhythm.* 11:492–501. https://doi.org/10.1016/j.hrthm.2013.11.026

Pezhouman, A., N. Singh, Z. Song, M. Nivala, A. Eskandari, H. Cao, A. Bapat, C.Y. Ko, T. Nguyen, Z. Qu, et al. 2015. Molecular basis of hypokalemia-induced ventricular fibrillation. *Circulation.* 132:1528–1537. https://doi.org/10.1161/CIRCULATIONAHA.115.016217

Qi, X., Y.H. Yeh, D. Chartier, L. Xiao, Y. Tsuji, B.J. Brundel, I. Kodama, and S. Nattel. 2009. The calcium/calmodulin/kinase system and arrhythmogenic afterdepolarizations in bradycardia-related acquired long-QT syndrome. *Circ. Arrhythm. Electrophysiol.* 2:295–304. https://doi.org/10.1161/CIRCEP.108.815654

Qu, Z., and D. Chung. 2012. Mechanisms and determinants of ultralong action potential duration and slow rate-dependence in cardiac myocytes. *PLoS One.* 7:e43587. https://doi.org/10.1371/journal.pone.0043587

Qu, Z., L.-H. Xie, R. Olcese, H.S. Karagueuzian, P.-S. Chen, A. Garfinkel, and J.N. Weiss. 2013. Early afterdepolarizations in cardiac myocytes: beyond reduced repolarization reserve. *Cardiovasc. Res.* 99:6–15. https://doi.org/10.1093/cvr/cvt104

Reed, M., C.C. Kerndt, and D. Nicolas. 2021. Ranolazine. *In* StatPearls. StatPearls Publishing. Treasure Island, FL.

Roden, D.M. 2016. Predicting drug-induced QT prolongation and torsades de pointes. *J. Physiol.* 594:2459–2468. https://doi.org/10.1113/JP270526

Rosen, M.R., A.L. Wit, and B.F. Hoffman. 1975. Electrophysiology and pharmacology of cardiac arrhythmias. VI. Cardiac effects of verapamil. *Am. Heart J.* 89:665–673. https://doi.org/10.1016/0002-8703(75)90514-1

Russell, R.P. 1988. Side effects of calcium channel blockers. *Hypertension.* 11:II42–II44. https://doi.org/10.1161/01.HYP.11.3_Pt_2.II42

Salari, S., M. Silverå Ejneby, J. Brask, and F. Elinder. 2018. Isopimaric acid - a multi-targeting ion channel modulator reducing excitability and arrhythmicity in a spontaneously beating mouse atrial cell line. *Acta Physiol. (Oxf.).* 222:e12895. https://doi.org/10.1111/apha.12895

Sánchez-Martínez, C., L.M. Gelbert, M.J. Lallena, and A. de Dios. 2015. Cyclin dependent kinase (CDK) inhibitors as anticancer drugs. *Bioorg. Med. Chem. Lett.* 25:3420–3435. https://doi.org/10.1016/j.bmcl.2015.05.100

Sanguinetti, M.C., and N.K. Jurkiewicz. 1992. Role of external Ca^{2+} and K^+ in gating of cardiac delayed rectifier K^+ currents. *Pflugers Arch.* 420:180–186. https://doi.org/10.1007/BF00374988

Sanguinetti, M.C., and M. Tristani-Firouzi. 2006. hERG potassium channels and cardiac arrhythmia. *Nature.* 440:463–469. https://doi.org/10.1038/nature04710

Sato, D., L.H. Xie, A.A. Sovari, D.X. Tran, N. Morita, F. Xie, H. Karagueuzian, A. Garfinkel, J.N. Weiss, and Z. Qu. 2009. Synchronization of chaotic early afterdepolarizations in the genesis of cardiac arrhythmias. *Proc. Natl. Acad. Sci. USA.* 106:2983–2988. https://doi.org/10.1073/pnas.0809148106

Schneider, C.A., W.S. Rasband, and K.W. Eliceiri. 2012. NIH Image to ImageJ: 25 years of image analysis. *Nat. Methods.* 9:671–675. https://doi.org/10.1038/nmeth.2089

Shimizu, W., T. Ohe, T. Kurita, M. Kawade, Y. Arakaki, N. Aihara, S. Kamakura, T. Kamiya, and K. Shimomura. 1995. Effects of verapamil and

propranolol on early afterdepolarizations and ventricular arrhythmias induced by epinephrine in congenital long QT syndrome. *J. Am. Coll. Cardiol.* 26:1299–1309. https://doi.org/10.1016/0735-1097(95)00313-4

Sicouri, S., L. Belardinelli, and C. Antzelevitch. 2013. Antiarrhythmic effects of the highly selective late sodium channel current blocker GS-458967. *Heart Rhythm.* 10:1036–1043. https://doi.org/10.1016/j.hrthm.2013.03.023

Skogestad, J., and J.M. Aronsen. 2018. Hypokalemia-induced arrhythmias and heart failure: New insights and implications for therapy. *Front. Physiol.* 9:1500. https://doi.org/10.3389/fphys.2018.01500

Soldatov, N.M. 1992. Molecular diversity of L-type Ca^{2+} channel transcripts in human fibroblasts. *Proc. Natl. Acad. Sci. USA.* 89:4628–4632. https://doi.org/10.1073/pnas.89.10.4628

Soldatov, N.M. 2012. Molecular determinants of Cav1.2 calcium channel inactivation. *ISRN Mol. Biol.* 2012:691341. https://doi.org/10.5402/2012/691341

Song, Y.H., H. Cho, S.Y. Ryu, J.Y. Yoon, S.H. Park, C.I. Noh, S.H. Lee, and W.K. Ho. 2010. L-type Ca^{2+} channel facilitation mediated by H_2O_2-induced activation of CaMKII in rat ventricular myocytes. *J. Mol. Cell. Cardiol.* 48: 773–780. https://doi.org/10.1016/j.yjmcc.2009.10.020

Song, L., D.W. Awari, E.Y. Han, E. Uche-Anya, S.H. Park, Y.A. Yabe, W.K. Chung, and M. Yazawa. 2015. Dual optical recordings for action potentials and calcium handling in induced pluripotent stem cell models of cardiac arrhythmias using genetically encoded fluorescent indicators. *Stem Cells Transl. Med.* 4:468–475. https://doi.org/10.5966/sctm.2014-0245

Song, L., S.E. Park, Y. Isseroff, K. Morikawa, and M. Yazawa. 2017. Inhibition of CDK5 alleviates the cardiac phenotypes in Timothy syndrome. *Stem Cell Reports.* 9:50–57. https://doi.org/10.1016/j.stemcr.2017.05.028

Stefani, E., and F. Bezanilla. 1998. Cut-open oocyte voltage-clamp technique. *Methods Enzymol.* 293:300–318. https://doi.org/10.1016/S0076-6879(98)93020-8

Szabo, B., R. Sweidan, C.V. Rajagopalan, and R. Lazzara. 1994. Role of Na^+:Ca^{2+} exchange current in $Cs(^+)$-induced early afterdepolarizations in Purkinje fibers. *J. Cardiovasc. Electrophysiol.* 5:933–944. https://doi.org/10.1111/j.1540-8167.1994.tb01133.x

Szentandrassy, N., D. Nagy, B. Hegyi, J. Magyar, T. Banyasz, and P. P Nanasi. 2015. Class IV antiarrhythmic agents: new compounds using an old strategy. *Curr. Pharm. Des.* 21:977–1010. https://doi.org/10.2174/1381612820666141029105910

Tazmini, K., M. Frisk, A. Lewalle, M. Laasmaa, S. Morotti, D.B. Lipsett, O. Manfra, J. Skogestad, J.M. Aronsen, O.M. Sejersted, et al. 2020. Hypokalemia promotes arrhythmia by distinct mechanisms in atrial and ventricular myocytes. *Circ. Res.* 126:889–906. https://doi.org/10.1161/CIRCRESAHA.119.315641

Wagner, S., H.M. Ruff, S.L. Weber, S. Bellmann, T. Sowa, T. Schulte, M.E. Anderson, E. Grandi, D.M. Bers, J. Backs, et al. 2011. Reactive oxygen species-activated Ca/calmodulin kinase IIδ is required for late $I_{(Na)}$ augmentation leading to cellular Na and Ca overload. *Circ. Res.* 108: 555–565. https://doi.org/10.1161/CIRCRESAHA.110.221911

Ward, C.A., and W.R. Giles. 1997. Ionic mechanism of the effects of hydrogen peroxide in rat ventricular myocytes. *J. Physiol.* 500:631–642. https://doi.org/10.1113/jphysiol.1997.sp022048

Weiss, J.N., A. Garfinkel, H.S. Karagueuzian, T.P. Nguyen, R. Olcese, P.S. Chen, and Z. Qu. 2015. Perspective: a dynamics-based classification of ventricular arrhythmias. *J. Mol. Cell. Cardiol.* 82:136–152. https://doi.org/10.1016/j.yjmcc.2015.02.017

Weiss, J.N., Z. Qu, and K. Shivkumar. 2017. Electrophysiology of hypokalemia and hyperkalemia. *Circ. Arrhythm. Electrophysiol.* 10:e004667. https://doi.org/10.1161/CIRCEP.116.004667

Wit, A.L. 2018. Afterdepolarizations and triggered activity as a mechanism for clinical arrhythmias. *Pacing Clin. Electrophysiol.* 41:883–896. https://doi.org/10.1111/pace.13419

Wu, M., H.V. White, B.A. Boehm, C.J. Meriney, K. Kerrigan, M. Frasso, M. Liang, E.M. Gotway, M.R. Wilcox, J.W. Johnson, et al. 2018. New Cav2 calcium channel gating modifiers with agonist activity and therapeutic potential to treat neuromuscular disease. *Neuropharmacology.* 131: 176–189. https://doi.org/10.1016/j.neuropharm.2017.12.022

Xie, L.H., F. Chen, H.S. Karagueuzian, and J.N. Weiss. 2009. Oxidative-stress-induced afterdepolarizations and calmodulin kinase II signaling. *Circ. Res.* 104:79–86. https://doi.org/10.1161/CIRCRESAHA.108.183475

Yang, L., J. Xu, E. Minobe, L. Yu, R. Feng, A. Kameyama, K. Yazawa, and M. Kameyama. 2013. Mechanisms underlying the modulation of L-type Ca^{2+} channel by hydrogen peroxide in guinea pig ventricular myocytes. *J. Physiol. Sci.* 63:419–426. https://doi.org/10.1007/s12576-013-0279-2

Yarotskyy, V., and K.S. Elmslie. 2007. Roscovitine, a cyclin-dependent kinase inhibitor, affects several gating mechanisms to inhibit cardiac L-type $(Ca_{(v)}1.2)$ calcium channels. *Br. J. Pharmacol.* 152:386–395. https://doi.org/10.1038/sj.bjp.0707414

Yarotskyy, V., G. Gao, B.Z. Peterson, and K.S. Elmslie. 2009. The Timothy syndrome mutation of cardiac CaV1.2 (L-type) channels: multiple altered gating mechanisms and pharmacological restoration of inactivation. *J. Physiol.* 587:551–565. https://doi.org/10.1113/jphysiol.2008.161737

Yarotskyy, V., G. Gao, L. Du, S.B. Ganapathi, B.Z. Peterson, and K.S. Elmslie. 2010. Roscovitine binds to novel L-channel (CaV1.2) sites that separately affect activation and inactivation. *J. Biol. Chem.* 285:43–53. https://doi.org/10.1074/jbc.M109.076448

Yazawa, M., B. Hsueh, X. Jia, A.M. Pasca, J.A. Bernstein, J. Hallmayer, and R.E. Dolmetsch. 2011. Using induced pluripotent stem cells to investigate cardiac phenotypes in Timothy syndrome. *Nature.* 471:230–234. https://doi.org/10.1038/nature09855

Zeng, J., and Y. Rudy. 1995. Early afterdepolarizations in cardiac myocytes: mechanism and rate dependence. *Biophys. J.* 68:949–964. https://doi.org/10.1016/S0006-3495(95)80271-7

Zhao, Z., H. Wen, N. Fefelova, C. Allen, A. Baba, T. Matsuda, and L.H. Xie. 2012. Revisiting the ionic mechanisms of early afterdepolarizations in cardiomyocytes: predominant by Ca waves or Ca currents? *Am. J. Physiol. Heart Circ. Physiol.* 302:H1636–H1644. https://doi.org/10.1152/ajpheart.00742.2011

Zühlke, R.D., G.S. Pitt, K. Deisseroth, R.W. Tsien, and H. Reuter. 1999. Calmodulin supports both inactivation and facilitation of L-type calcium channels. *Nature.* 399:159–162. https://doi.org/10.1038/20200
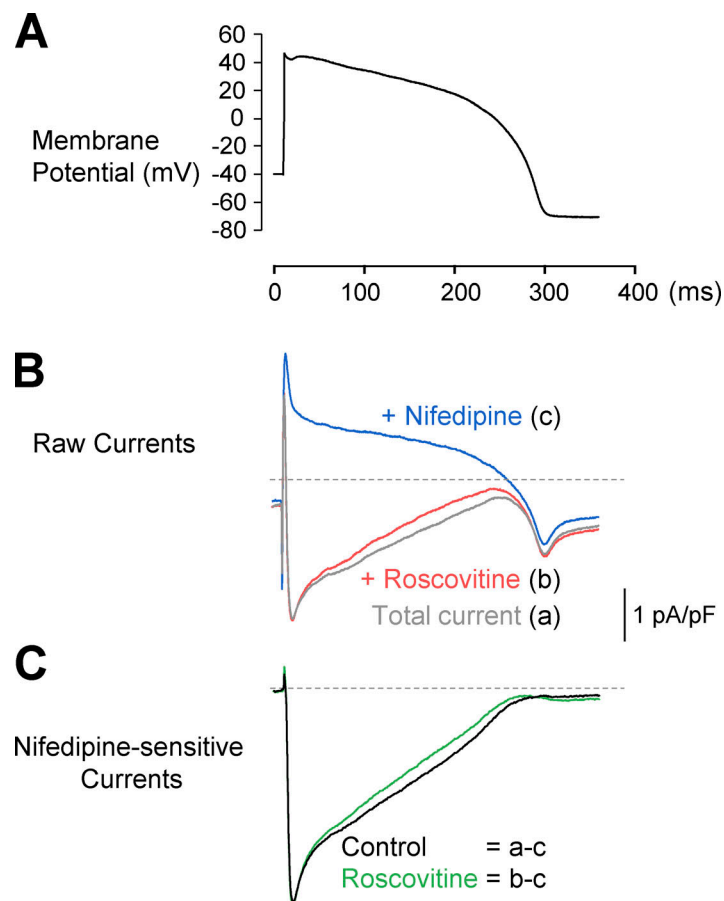
Supplemental material

Figure S1. **Experimental and analytical procedure to isolate nifedipine-sensitive current under AP clamp. (A)** AP waveform used as voltage command in AP-clamp recordings shown in B. **(B)** Three sequential recordings from the same myocyte under ionic conditions suitable for Ca^{2+} current recording. In gray is the total current measured before the sequential addition of 20 µM roscovitine (red) and 10 µM nifedipine (blue). The selective effect of roscovitine on the late current is already evident in the raw, unsubtracted current density. **(C)** The difference in current density obtained by subtracting from the total current (B, gray) and from roscovitine (B, red) recordings of the residual nifedipine-insensitive current (B, blue) is shown.
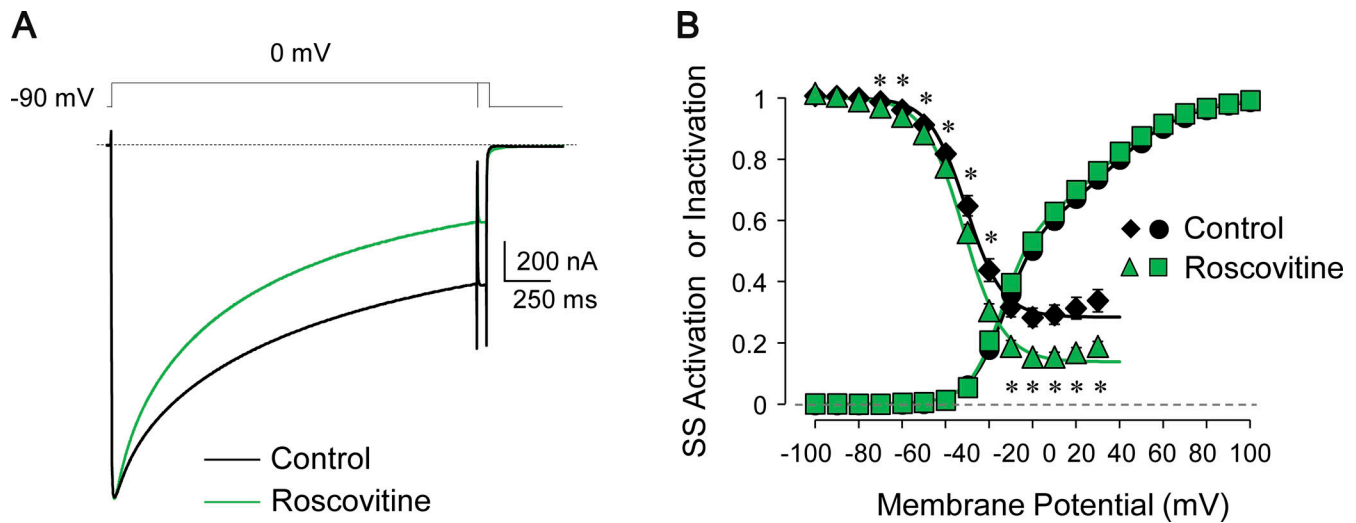
Figure S2. **Roscovitine reduces late I_{Ca,L} (noninactivating component) in human Ca_V1.2 channels. (A)** Superimposed Ba^{2+} currents from Ca_V1.2 channels expressed in oocytes ($\alpha_{1C} + \beta_{2b} + \alpha_2\delta - 1$) before (control) and after 100 μM roscovitine. **(B)** Average steady-state (SS) activation and quasi–steady-state inactivation curves obtained before and after roscovitine extracellular application. Continuous lines are Boltzmann fits to the activation and inactivation data points (fitting parameters are reported in Table S2). Note that roscovitine selectively reduced the late I_{Ca,L}, enhancing the extent of the steady-state inactivation (i.e., reduced pedestal of the steady-state inactivation curve, black diamond versus green triangle) without affecting the voltage dependence of activation (black circle versus green square). Data points are mean ± SEM; n = 7; *, P < 0.05.
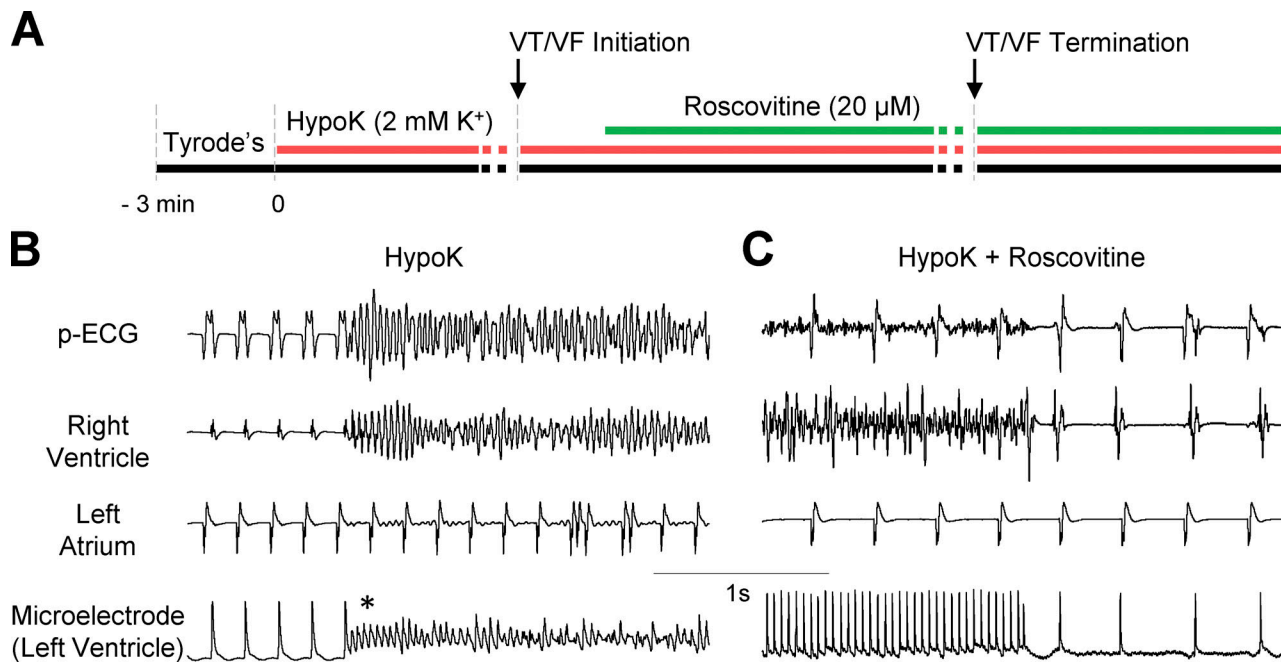

Figure S3. **Roscovitine suppresses hypokalemia-induced VT/VF in young rat hearts. (A)** Experimental protocol used to test the ability of roscovitine to suppress VT/VF in ex vivo perfused young rat hearts. **(B and C)** Bipolar electrograms and microelectrode recordings from the indicated chambers of the heart. p-ECGs were obtained from right atrial–left ventricular leads. Single-cell APs were measured by a glass microelectrode inserted in the left ventricle epicardium. **(B)** The recordings show the initiation of VF after 12 min of exposure to hypokalemia (HypoK; Tyrode's with 2 mM K$^+$). Note the initiation of VF by cellular EAD-mediated triggered activity, which arose suddenly during sinus rhythm (microelectrode, *). **(C)** Recordings from the same heart as in B, showing suppression of VF 8 min after the addition of roscovitine (20 μM) to the perfusate in the continuous presence of hypokalemia.
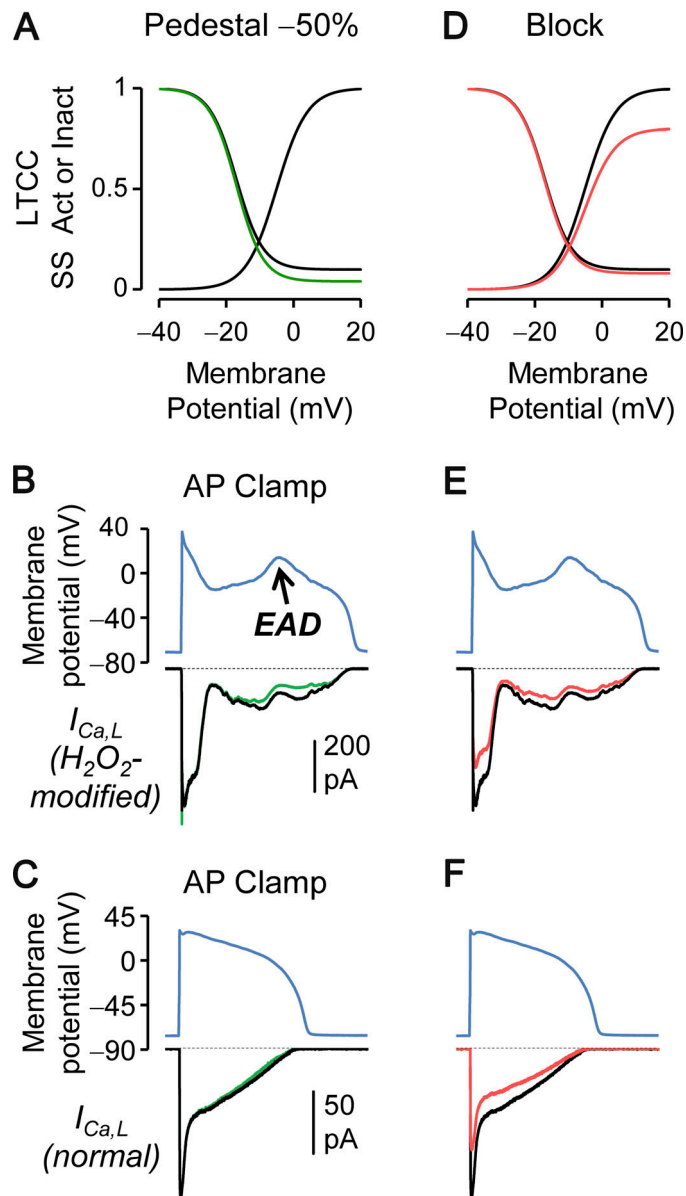
Angelini et al.
Ca_V1.2 gating modification as antiarrhythmic strategy

Journal of General Physiology   S2
https://doi.org/10.1085/jgp.202012584

Figure S4. **I$_{Ca,L}$ pedestal reduction selectively reduces late versus peak I$_{Ca,L}$, unlike class IV antiarrhythmics. (A)** LTCC steady-state (SS) activation (Act) and inactivation (Inact) curves. The green inactivation curve demonstrates a 50% reduction of I$_{Ca,L}$ pedestal. **(B)** The UCLA myocyte model (Mahajan et al., 2008) was modified to accept membrane potential input as in our previous dynamic-clamp studies (Madhvani et al., 2011; Madhvani et al., 2015). In addition, its LTCC parameters were modified to simulate the channel under oxidative stress conditions. The model was "voltage-clamped" with the AP waveform from an isolated rabbit ventricular myocyte under oxidative stress, exhibiting an EAD and increased AP duration (blue). The black current trace is the UCLA model I$_{Ca,L}$ output produced by the blue AP without further modification; the green current is the UCLA model current output with 50% reduced pedestal (as in A and Madhvani et al., 2015). Under EAD-favoring conditions, pedestal reduction (green) results in marked decrease of I$_{Ca,L}$ flowing in phases 2 or 3 of the AP (late I$_{Ca,L}$) but did not affect peak I$_{Ca,L}$ flowing after the AP upstroke. **(C)** As above for the UCLA model under normal (non-oxidative stress) conditions clamped by a normal AP waveform (blue). Pedestal reduction (green current) does not affect I$_{Ca,L}$. **(D)** The LTCC steady-state activation and inactivation curves were modified to simulate 20% blockade (red; as in class IV antiarrhythmics). **(E and F)** As in B and C. Red current represents the UCLA I$_{Ca,L}$ output with 20% blockade under EAD-favoring (E) or normal (F) conditions. Note that blockade indiscriminately reduced both peak (red arrow) and late I$_{Ca,L}$, which in turn would result in negative inotropy (Godfraind, 2017; Karagueuzian et al., 2017). By contrast, pedestal reduction (green current in B and C) preserved peak I$_{Ca,L}$, so it follows that Ca^{2+} release and cell shortening would be unaffected.

Provided online are two tables. Table S1 lists I$_{Ca,L}$ fitting parameters of steady-state activation and inactivation in ventricular myocytes. Table S2 presents fitting parameters of steady-state activation and inactivation.

Angelini et al.
Ca$_V$1.2 gating modification as antiarrhythmic strategy

Journal of General Physiology   S3
https://doi.org/10.1085/jgp.202012584